Targeting DNA damage and repair mechanism in FLT3-ITD acute myeloid leukemia – a mechanistic and therapeutic study

Ng, Ka Lam

Awarding institution:
King's College London

TARGETING DNA DAMAGE AND REPAIR MECHANISM IN FLT3-ITD ACUTE MYELOID LEUKEMIA – A MECHANISTIC AND THERAPEUTIC STUDY

NG, KA LAM

Ph.D. THESIS

KING'S COLLEGE LONDON

DECEMBER 2018

Abstract of thesis entitled

Targeting DNA damage and repair mechanism in FLT3-ITD acute myeloid leukemia - a mechanistic and therapeutic study

Submitted by

NG, Ka Lam

for the Degree of Doctor of Philosophy

at King's College London

December 2018

Internal tandem duplication (ITD) of fms-like tyrosine kinase 3 (*FLT3*) is one of the most common mutations in acute myeloid leukemia (AML), occurring in nearly 30% of cases. FLT3-ITD involves in-frame duplication of 3-400 base-pairs at the juxta-membrane, resulting in ligand-independent activation of FLT3 signaling. Downstream effectors include activation of STAT5 via SRC kinase, phosphorylation of FOXO3A, down-regulation of the equilibrative nucleoside transporter 1 (ENT1) for cytarabine, and induction of reactive oxygen species (ROS) production. These aberrant signals result in increased DNA damage and defective repair, increased cellular proliferation and resistance to apoptosis.

Induction of ROS and DNA damage in FLT3-ITD AML has led to investigation of their mechanistic link and exploration of potential therapeutic targets. By examining gene expression associated with DNA repair in primary AML samples, *BRCA2* expression was shown to be down-regulated in FLT3-ITD AML when compared with AML with wild-type FLT3 as well as normal hematopoietic cells. BRCA2 is an important protein in mediating homologous recombination (HR), providing a possible explanation for defective DNA damage response (DDR) in this AML subtype. A

double-stranded break (DSB) DNA repair assay was used to measure the fidelity of DSB repair, either via error-free HR or error-prone non-homologous end joining (NHEJ). The results showed that HR was down-regulated in murine Ba/F3 cells transduced with FLT3-ITD while NHEJ remained active.

DDR pathway as a target for therapeutic intervention in human cancers is exemplified by the use of poly (ADP-ribose) polymerase (PARP) inhibitor (PARPi) in *BRCA* mutant breast and ovarian cancers. In Ba/F3 FLT3-ITD cells and knockin *Flt3* $^{ITD/+}$ *Npm1* $^{c/+}$ mouse leukemic cells, PARPi Olaparib suppressed leukemia growth *in vitro*. Combination of chemotherapy and Olaparib worked synergistically to eradicate leukemic cells in MOLM-13 murine xenograft model. Biochemically, Olaparib inhibited base excision repair and increased the DSB damage. Olaparib also increased intracellular ROS, resulting in positive feedback that accentuated DNA damage. To identify potential therapeutic targets that may be exploited in combination treatment with Olaparib, a DDR *shRNA* library screening was performed. Potential candidate genes included those associated with checkpoint factors and DNA replication factors, for instance, Atr kinase and members of the Family B DNA Polymerase.

In summary, FLT3-ITD AML showed defective HR and higher levels of intracellular ROS and DSB, and Olaparib induced genomic instability and apoptosis. Targeting defective DNA repair in FLT3-ITD AML using PARPi might be considered as a novel therapeutic strategy.

Declaration

I declare that this thesis represents my own work, except where due acknowledgement is made, and that has not been previously included in a thesis, dissertation or report submitted to this University or to any other institution for a degree, diploma or other qualifications.

Signed…… 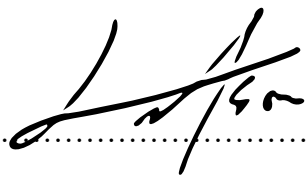 ……

NG, Ka Lam

Acknowledgements

I would like to express my sincerest gratitude to my supervisors, Prof. Anskar Y. H. Leung and Prof. Eric C. W. So. It has been a value experience to learn the perspectives and importance of leukemia research from clinical and basic science studies.

I would like to thank my dearest friends and labmates in HKU: Dr. Alvin Ma, Dr. Himm Man, Dr. Alex He, Dr. Yuhan Guo, Dr. Xiangguo Shi, Dr. Christa Ho, Dr. Eric Ho, Dr. Stephen Lam, Dr. Qingyun Wu, Dr. Ning Yang, Dr. Wan Liu, Miss Chae yin Cher, Mr. Harry Wong, Miss Toni Man, Miss Bowie Cheng, Mr. Leo Kan, Mr. Siyang Wang, Miss Lulu Wang, and friends and labmates in KCL: Dr. Bernd Zeisig, Miss Amanda Wilson, Dr. Michael Cheung, Dr. Tsz Kan Fung, Dr. Priscilla Lau, Dr. Rick Kong, Dr. Jackie Chen, Dr. Marco Saia, Dr. Lu Zhao, Dr. Jennifer Lynch, Dr. Haoli Li, Dr. Yongrang Kim, Dr. Bohan Stanojevic, Mr. Ray Tsai, Miss Siyi Zhang, Miss Claire Lynn and Mr. Mickey Wong for their continuous support and inspiration. In particular, my sincere thanks to Miss Claire Lynn for her help with bioinformatics analysis of the *shRNA* screening.

I would like to thank Dr. Jerome Tamburini (Institut Cochin, Université Paris Descartes, Paris, France) for providing the Ba/F3 FLT3-ITD cell line, Dr. Johannes Zuber's group (Research Institute of Molecular Pathology, Vienna) for sharing their latest protocol on *shRNA* library screening and Dr. George S Vassiliou (Sanger Institute, UK) for providing the *Flt3* $^{ITD/+}$ *x Npm1* $^{c/+}$ leukemic cells.

Last but not least, I would like to express my deepest gratitude to my family and friends for their continuous support and encouragement.

List of Publications and Award

Publications with my contribution during the PhD study:

1. Man, C. H., Fung, T. K., Wan, H., Cher, C. Y., Fan, A., **Ng, N**., Ho, C., Wan, T. S., Tanaka, T., So, C. W., Kwong, Y. L. & Leung, A. Y. Suppression of SOX7 by DNA methylation and its tumor suppressor function in acute myeloid leukemia. *Blood* **125**, 3928-3936, doi:10.1182/blood-2014-06-580993 (2015).

2. Hou, J., Luo, T., **Ng, K. L**., Liang, R., Leung, A. Y. & Sun, D. Characterization of drug effect on leukemia cells through single cell assay with optical tweezers and dielectrophoresis. *IEEE Trans Nanobioscience*, doi:10.1109/TNB.2016.2616160 (2016).

3. Lam, S. S., Ho, E. S., He, B. L., Wong, W. W., Cher, C. Y., **Ng, N. K**., Man, C. H., Gill, H., Cheung, A. M., Ip, H. W., So, C. C., Tamburini, J., So, C. W., Ho, D. N., Au, C. H., Chan, T. L., Ma, E. S., Liang, R., Kwong, Y. L. & Leung, A. Y. Homoharringtonine (omacetaxine mepesuccinate) as an adjunct for FLT3-ITD acute myeloid leukemia. *Sci Transl Med* **8**, 359ra129, doi:10.1126/scitranslmed.aaf3735 (2016).

Awards:

1. Poster presentation award, Cancer Studies PhD symposium 2017, Kings College London

List of Figures

Appendix

List of abbreviations

Abbreviation	Full name
2HG	D-2-hydroxyglutarate
8-OHdG	8-hydroxy-2'-deoxyguanosine
8-oxoG	8-hydroxyguanine
a-KG	alpha-ketoglutarate
Alt-NHEJ	alternative nonhomologous end-joining
AML	acute myeloid leukemia
APL	acute promyelocytic leukemia
ATM	ataxia telangiectasia mutated
Atr	ATM and rad3-related
BER	base excision repair
BM	bone marrow
cDNA	complementary DNA
CG	cytogenetic
ChIP	chromatin immunoprecipitation
CML	chronic myelogenous leukemia
CMML	chronic myelomonocytic leukemia
D2HG	D-2-hydroxyglutarate
DDR	DNA damage response
dGFP	defective GFP
Diff.	difference
DMSO	dimethylsulfoxide
DNA-PKcs	DNA-dependent protein kinase catalytic subunit
DR	DNA repair
DSB	double-stranded break
DSBR	double stranded breaks repair
ENT1	equilibrative nucleoside transporter 1
FA	fanconi anemia
FapyG	formamidopyrimidines
FBS	fetal bovine serum
FLT3	fms-like tyrosine kinase 3
γ–H2AX	gamma-H2AX
H2DCFDA	2'7'-dichlorodihydro-fluorecein diacetate
HBSS	Hanks' Balanced Salt Solution
HR	homologous recombination
HSCT	haematopoietic stem cell transplantation
HSPC	hematopoietic stem and progenitor cells
IDH1	isocitrate dehydrogenase 1
IDH2	isocitrate dehydrogenase 2
ITD	Internal tandem duplication
LIG3	DNA ligase IIIα

LSC	leukemia stem cell
MDS	myelodysplastic syndrome
MMEJ	microhomology-mediated end joining
MMR	mismatch repair
MNC	mononuclear cell
MRE11	meiotic recombination 11 homolog A
MRN	MRE11/RAD50/NSB1
NAC	N-acetyl cysteine
NAPDH	*nicotinamide adenine dinucleotide phosphate-oxidases*
NER	*nucleotide excision repair*
NHEJ	non-homologous end joining
NOX4	NAPDH oxidase 4
NSG	NOD/SCID/IL2Rg$^{-/-}$
Ola.	Olaparib
ORF	open reading frame
PARP	poly (ADP-ribose) polymerase
PARPi	PARP inhibitor
PB	peripheral blood
PBSC	peripheral blood stem cell
Pdrop	probability of hairpin dropout
Pdrop of O-V	probability of hairpin dropout of Olaparib-treated minus vehicle
pHi	intracellular pH
phox	phagocytic oxidase
ROS	reactive oxygen species
RTK	receptor tyrosine kinase
SDS-PAGE	sodium dodecyl sulfate polyacrylamide gel electrophoresis
SOP	standard operating procedure
SSB	single-stranded break
TKD	tyrosine kinase domain
TLR	Traffic Light Reporter
TLS	translesion repair
TP53BP1	p53-binding protein 1
Veh.	vehicle
WB	Whole Blood
WHO	World Health Organization

Table of Contents

Chapter 1. Introduction

1.1 Background of acute myeloid leukemia

Acute myeloid leukemia (AML) is a heterogeneous group of diseases with diverse clinicopathologic features, cytogenetic (CG) abnormalities and genetic mutations, sharing in common an abnormal increase in myeloblasts in peripheral blood (PB) and bone marrow (BM) [1]. According to the World Health Organization (WHO) classification, diagnosis of AML is defined by the presence of more than 20% myeloblasts either in the BM or PB, with the exception of t(8;21), inv(16) and t(15;17) in which the presence of specific CG abnormalities are sufficient for diagnosis [2].

Despite the heterogeneity, treatment of AML has been uniform and unchanged in the past 4 decades [3-6]. Induction chemotherapy, known as the "7+3" regimen, comprises concurrent treatment with cytarabine (day 1-7) and daunorubicin or equivalence (day 1-3). Following an initial remission (blasts ≤ 5%), patients receive either consolidation chemotherapy (high dose cytarabine) or allogeneic haematopoietic stem cell transplantation (HSCT). However, disease relapse is a major cause of treatment failure and only 30-40% can survive long-term. For elderly patients unfit for conventional treatment, the outcome is dismal [7]. There is an urgent need to improve treatment outcome.

1.2 Aberrant DNA damage repair mechanism in myeloid malignancies

1.2.1 Introduction

Our genomic DNA is constantly exposed to genotoxic stress such as replication errors, reactive oxidative species (ROS) and ultraviolet radiation (Fig 1.1) [8]. Single-strand DNA breaks (SSB) are repaired by base excision repair (BER), nucleotide excision repair (NER) and mismatch repair (MMR) [9]. If unrepaired, SSB or crosslinks can induce replication fork collapse and result in double-stranded break (DSB) during DNA replication [10-12]. Cancer therapies such as ionization radiation, alkylating agents, topoisomerase II inhibitors or excessive ROS may also induce DSB [13,14]. DNA damage response (DDR) is strictly regulated to maintain genomic integrity and protect cells from genomic stress [15]. When DNA damage occurs, cells respond by an orchestrated network of signals that sense and repair the damage. At the same time, cell-cycle checkpoints are activated to allow time for DDR and avoid inadvertent replication of damaged DNA. If the damage is not repaired, these checkpoints can trigger cellular senescence or apoptosis [16,17] .

1.2.2 DSB repair mechanism in mammalian cells

Three major repair pathways of DSB have been described in mammals, viz. BRCA-mediated error-free homologous recombination (HR), DNA-dependent protein kinase (DNA-PK)-mediated error-prone non-homologous end joining (NHEJ) and a less characterized microhomology-mediated end joining (MMEJ) (Fig. 1.2) [8,14,18]. HR uses

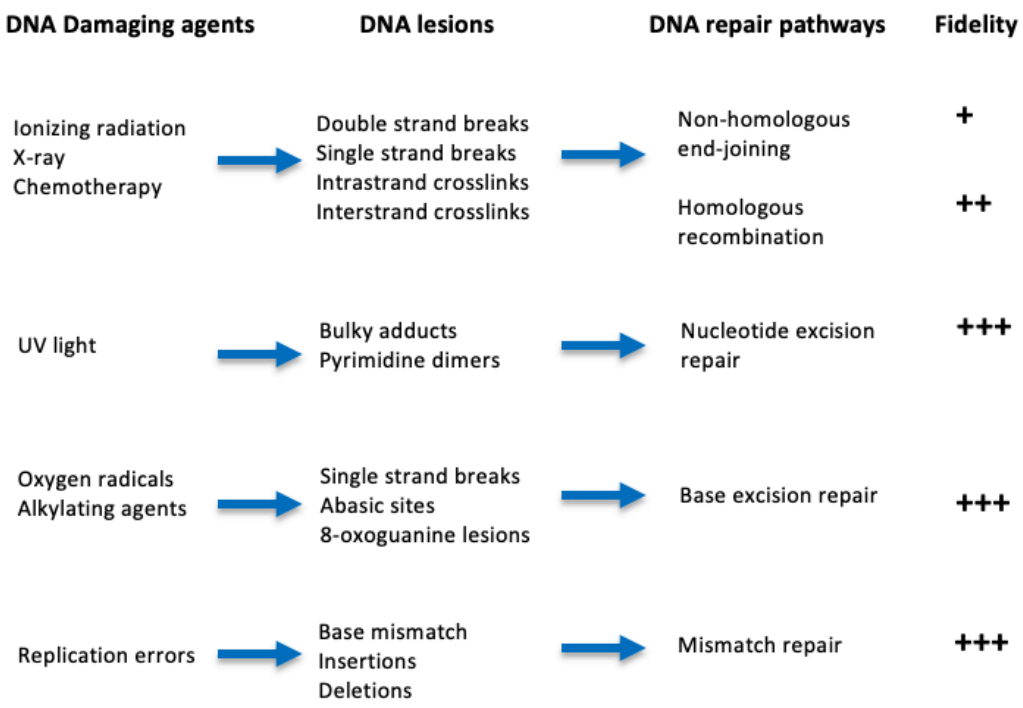

Figure 1.1 Examples of DNA damage response pathways in mammalian cells. DNA damage agents induce a spectrum of DNA lesions, which can be repaired by distinct and specific DNA repair pathways with various degrees of fidelity. The diagram is adapted from [19].

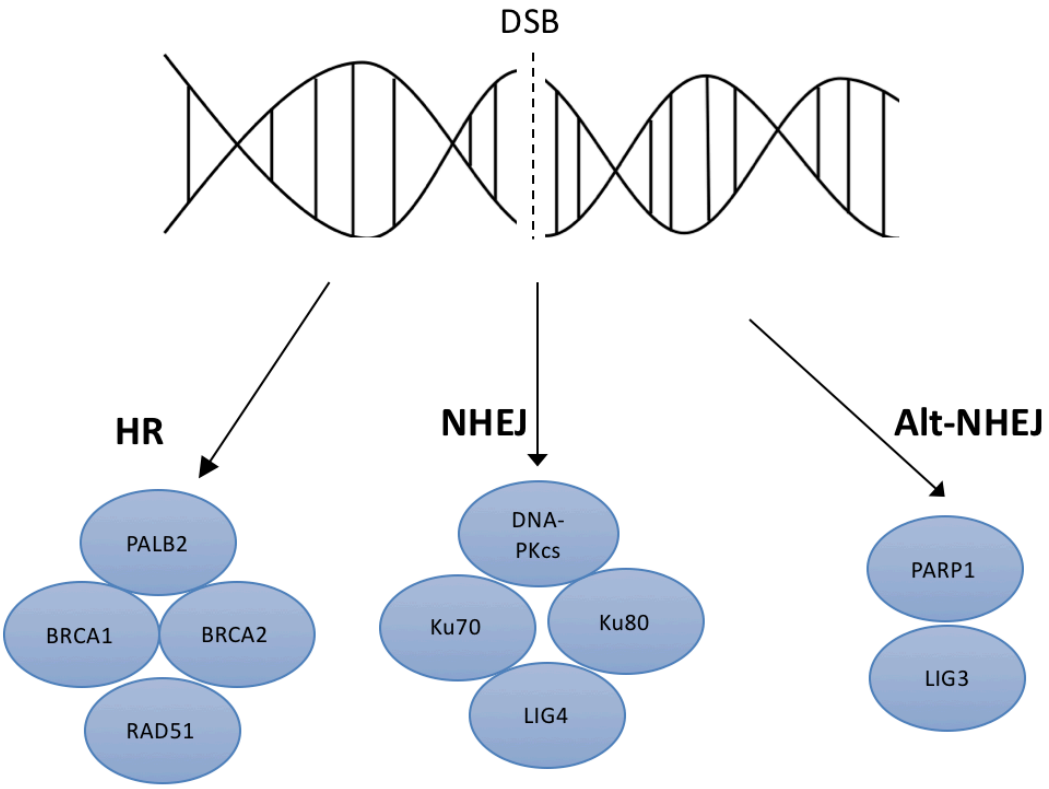

Figure 1.2. DSB repair pathways in mammalian cells.

DNA double-stranded breaks can be repaired by 3 major pathways, including homologous recombination (HR), non-homologous end joining (NHEJ) and alternative non-homologous end joining (Alt-NHEJ). Key components of these pathways are illustrated in the diagram. The diagram is adapted from [20].

sister chromatid as template for accurate DSB repair and is only active in proliferating cells during late S and G2 phases of cell cycle. NHEJ occurs throughout cell cycle but mostly during G1 in both proliferating and quiescent cells [21]. Emerging evidences demonstrate a PARP1-dependent and microhomology-mediated end joining (MMEJ), also known as alternative nonhomologous end joining (Alt-NHEJ) [22]. Mechanistically, MMEJ and HR share the same MRE11-dependent initial end resection step and both repair pathways occur during S/G2 phase of cycle [23].

DSBs are rapidly detected by the MRE11/RAD50/NSB1 (MRN) complex or the Ku70/80 complex, followed by phosphorylation and activation of the apical sensor kinases ataxia telangiectasia mutated (ATM) and DNA-dependent protein kinase catalytic subunit (DNA-PKc) respectively [24]. Activated apical sensor kinases phosphorylate the serine139 residue of histone variant gamma-H2AX (γ–H2AX) at the DSB site. Subsequently, DNA damage mediators are recruited, for instance, TP53-binding protein 1 (TP53BP1) in NHEJ and BRCA1 in HR [25,26]. Defective DDR has been shown to play an important role in the pathogenesis of myeloid malignancies driven by *BCR-ABL* fusion and *NRAS* activating mutations[18,27-39] and more recently in AML carrying *IDH1/2* mutations and specific gene function arising from translocation [40-42].

1.2.3 DNA repair defect in chronic myelogenous leukemia

Defective DDR has been reported in chronic myelogenous leukemia (CML) [31,35,36]. CML is caused by a balanced translocation between chromosome 9 and 22, resulting in the formation of oncogenic fusion protein BCR-ABL [36]. The latter is a constitutively active tyrosine kinase that activates cell proliferation and protects them from apoptosis

[35]. Recent reports showed that it also induced ROS production and caused DSB and genomic instability [31-34]. On the other hand, DDR by HR was defective in CML cells [27,28,33]. Mutation analysis of HR related proteins showed that half of them belonged to G/C → A/T transitions, suggesting oxidative DNA damage due to ROS [43].

1.2.4 RAS are responsible for elevated ROS and DNA damage in myeloid malignancies

Activating *NRAS* and *KRAS* mutations at codons 12, 13 and 61 have been shown to compromise its GTPase activity, leading to a constitutively active and GTP-bound state [38]. *N- & K-RAS* mutations, mostly at codons 12 and 13 occur in 66% of chronic myelomonocytic leukemia (CMML) [39] whereas 30% of AML carry *NRAS mutations* [38] . Overexpression of *NRAS-G12D* and *BCL2* driven by *MRP8* promoter in a double transgenic mouse model led to increase in DNA damage and NHEJ repair errors [37]. RAC1, an essential component of the NADPH oxidase complex, was required for ROS production in the *NRAS/BCL2* mice. Mechanistically, RAC1 was a downstream target of RAS activation [44]. DSB and NHEJ repair error could be ameliorated by feeding the mice with anti-oxidant N-acetyl cysteine (NAC), a scavenger of ROS, suggesting that the RAS/RAC1 pathways and ROS could be a therapeutic target for RAS mutated myeloid malignancies.

1.2.5 IDH1/2 mutation impairs homologous recombination

Isocitrate dehydrogenase 1 and 2 (*IDH1/2*) are frequently mutated in AML and myelodysplastic syndrome (MDS). Wild-type IDHs catalyze oxidative decarboxylation of isocitrate to alpha-ketoglutarate (α-KG) in citric acid cycle. Mutations of *IDH1* at codon 132 and *IDH2* at codon 140 and 172 conferred new

substrate specificity and enzyme activity and the mutant enzymes converted α-KG to the oncometabolite D-2-hydroxyglutarate (2HG) [45,46]. The latter inhibited TET family proteins, thereby impeding DNA methylation [45]. In *idh1*-R132Q knockin mouse model, the mutant *idh1* down-regulated *Atm* by altering histone methylation, impairing DNA repair via a TET2-independent pathway [42]. Recently, *IDH1 R132H* and *IDH2 R172K* knockin cell lines showed defective HR and increased sensitivity to PARP inhibitor (PARPi), reminiscent of synthetic lethality in *BRCA1/2* mutant breast and ovarian cancers [40]. The phenotype could be restored by inhibitors against mutant IDH1, proving the pathogenetic role of mutant IDH1/2 in defective DDR.

1.2.6 HR deregulation in translocations involving transcription factors

Chromosomal translocation resulting in fusion genes with aberrant transcription factor function is a common feature in AML [1]. RUNX1-RUNX1T1 and PML-RARα fusion proteins have been shown to suppress expression of key HR-associated genes and hence defective HR [41]. Mouse leukemic cells carrying these fusions were sensitive to PARPi, in contrast to those carrying *MLL-AF9* fusion. Mechanistically, Hoxa9 that was downstream to MLL-AF9, activated expression of HR-associated genes. Pharmacological inhibition or genetic knockout of *Hoxa9* gene impaired DDR and re-sensitized MLL-AF9 leukemic cells to PARPi. Moreover, combination of PARPi with DNMT inhibitors or chemotherapies showed significant anti-leukemic effects in both mouse and human leukemia cells carrying *MLL-AF9*, providing important leads for clinical trials [47].

1.3 The role of internal tandem duplication of Fms-Like Tyrosine kinase 3 in AML

1.3.1 Introduction to Fms-Like Tyrosine kinase 3

Fms-like tyrosine kinase 3 (*FLT3*) encodes a 933-amino-acids class III receptor tyrosine kinase (RTK) and is located on chromosome 13q12, consisting of 24 exons [48,49]. *FLT3* is preferentially expressed in human CD34+ hematopoietic stem and progenitor cells (HSPC) where it provides signals for survival, proliferation and differentiation. The FLT3 receptor comprises i) five extracellular immunoglobulin-like domain for ligand binding and receptor dimerization in the N-terminus; ii) a transmembrane domain; iii) a juxtamembrane domain; and iv) two intracellular tyrosine kinase domains (TKD1 and TKD2) at the C-terminus (Fig. 1.3) [50,51]. FLT3 protein undergoes glycosylation in endoplasmic reticulum and Golgi apparatus to promote its translocation to the cell membrane [52,53]. Upon binding to its ligand, FLT3 undergoes dimerization, auto-phosphorylation and activation of the downstream effectors including PI3K (phosphoinositide-3-kinase), JAK-STAT and RAS pathways (Fig. 1.4) [54-56].

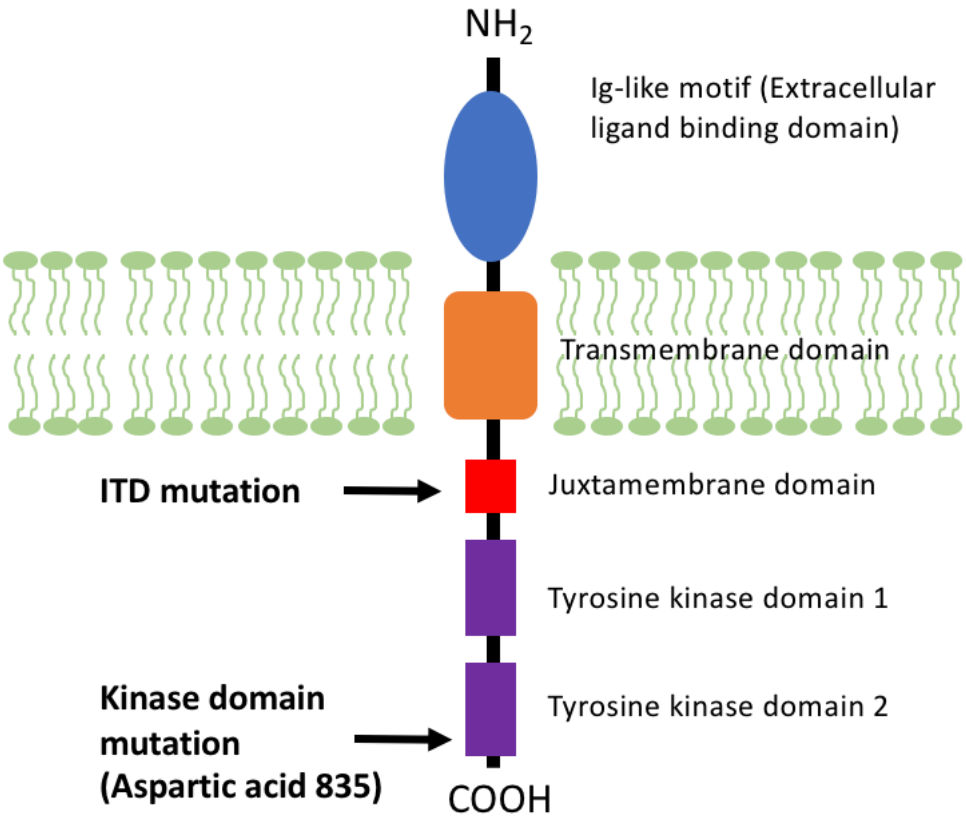

Figure 1.3 A schematic diagram of the human FLT3 receptor tyrosine kinase. The positions of internal tandem duplication (ITD) mutation and tyrosine kinase domain (TKD) mutations are as indicated.

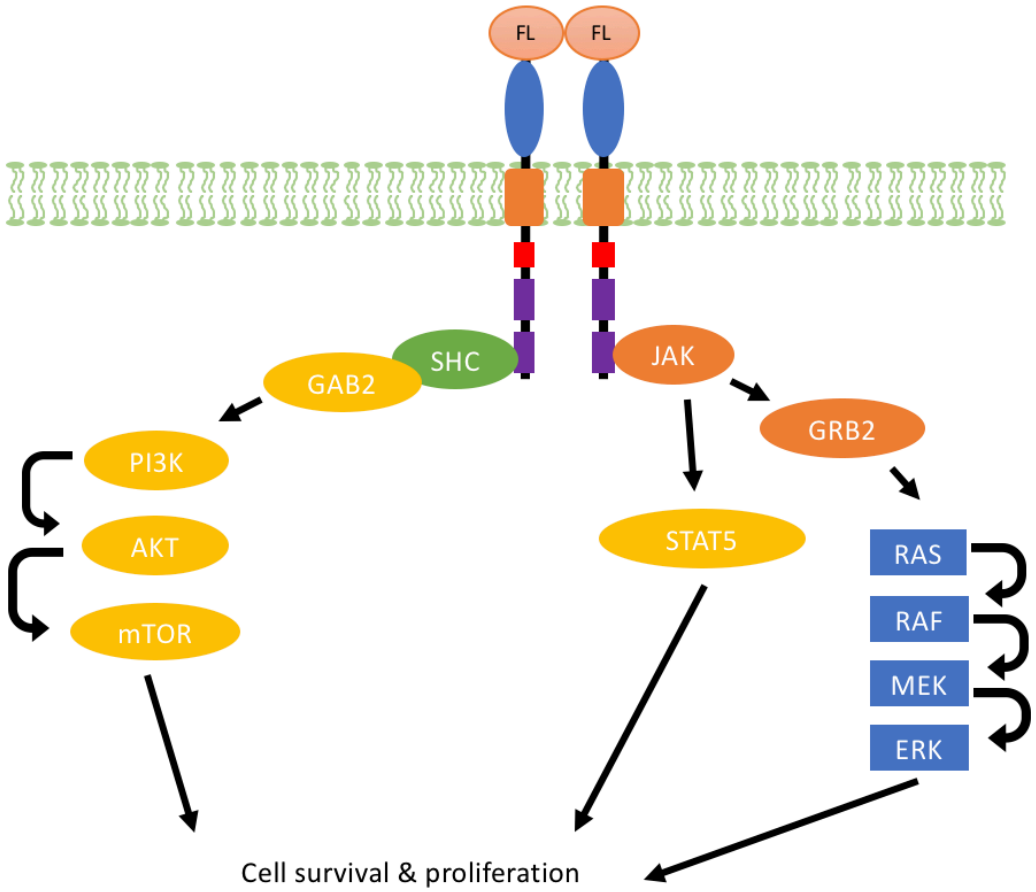

Figure 1.4 A schematic diagram showing downstream signaling that occurred upon activation of FLT3.

The binding of the FLT3 ligand (FL) to the receptor triggered the formation of FLT3 homodimer. The activation of FLT3 induced signal transduction via PI3K (phospatidylinositol-3-kinase), JAK-STAT and RAS pathways, resulting in enhanced cell survival and proliferation.

1.3.2 Internal tandem duplication of Fms-Like Tyrosine kinase 3

Internal tandem duplication (ITD) of *FLT3* is one of the most common mutations in AML, particularly in AML with normal cytogenetics, t(6;9) translocation and acute promyelocytic leukemia (APL) [57]. FLT3-ITD involves in-frame duplication of 3-400 base-pairs at the juxta-membrane or TKD1 domains, resulting in constitutive activation of FLT3 signaling independent of its ligand. Downstream effectors of FLT3 include activation of STAT5 via SRC kinase, phosphorylation of FOXO3A, down-regulation of the equilibrative nucleoside transporter 1 (ENT1) for cytarabine, and induction of ROS production. These aberrant signals result in increased cellular proliferation, resistance to apoptosis and defective DDR. FLT3-ITD AML showed higher relapse risk after conventional treatment and hence inferior outcome. Larger size of ITD, higher allelic burden and multiple ITD mutations also indicated worse prognosis [58-60].

1.3.3 Clinical strategies to prolong remission are lacking

Clinical trials using multi-kinase or specific FLT3 inhibitors including sorafenib and quizartinib (formerly AC220) have been effective in clearing myeloblasts from PB and BM but responses are typically transient. Proposed mechanisms of drug resistance include emergence of TKD mutations (*FLT3/ITD/TKD*) [61,62], over-expression of FLT3 signaling proteins [63], protection of leukemia stem cells (LSC) in niche [64] and an increase in intracellular pH (pHi) [65]. Effective means to overcome drug resistance is presently lacking.

1.4 Aberrant DNA damage response signaling in FLT3-ITD AML

1.4.1 Elevated intracellular ROS is the cause of genomic instability in FLT3-ITD AML

FLT3-ITD has been shown to induce ROS production. The latter induced DNA damages, including oxidization of DNA bases and abasic sites as well as single and double-stranded DNA breaks[66]. In particular, guanine was most sensitive to oxidation by ROS due to its low redox potential [67], forming 8-hydroxyguanine (8-oxoG) which was a highly mutagenic [68]. Increase in ROS was closely related to the NOX family of nicotinamide adenine dinucleotide phosphate-oxidases (NAPDH oxidases, NOXs). There were 7 isoforms designated as NOX1-5 and dual oxidase 1-2 (DUOX1-2), whereas *NOX2* and *NOX4* are expressed in leukemia [44,69]. Each NOX enzymatic complex comprised 6 subunits, including a GTPase, usually RAC1 or RAC2 and 5 phox units (phagocytic oxidase) including $gp91^{phox}$, $p22^{phox}$, $p40^{phox}$, $p47^{phox}$ and $p67^{phox}$[70]. Mechanistically, a direct association of phosphorylated STAT5 (P-STAT5) to RAC1-GDP has been shown to keep the GTPase in its active state, providing a possible mechanism for increased ROS generation. In addition, FLT3-ITD signaling stabilized $p22^{phox}$ protein via AKT signaling and P-STAT5 can activate transcription of *NOX4* [71,72]. The resulting increase in NOX4 protein generates ROS that caused damage to genomic DNA. The myeloblast-like 32D cell line expressing *FLT3-ITD* had a higher level of oxidized DNA 8-hydroxy-2'-deoxyguanosine (8-OHdG) and DSBs than its wild-type counterparts. Mechanistically, FLT3-ITD increased both NOX and $p22^{phox}$ protein expression level. Most importantly, NOX4, $p22^{phox}$ and FLT3-ITD protein had been shown to co-localize in the nuclear membrane and were essential for the generation of H_2O_2 that diffused into the nucleus to damage genomic DNA[72]. The reported mechanism of ROS generation via FLT3-ITD signaling is illustrated in Figure 1.5.

Furthermore, increased ROS might oxidase and hence inactivate a tumour suppressor protein-tyrosine phosphatase PTP/DEP-1 which was a negative regulator of FLT3 signaling. Therefore, ROS may feed forward to FLT3-ITD signaling by inactivating its negative regulator. In this context, *NOX4* has been shown to be particularly relevant [73]. *NOX4* knockdown by *shRNA* reduced ROS, restored PTP/DEP-1 activity and attenuated FLT3-ITD cells proliferation *in vitro*. A NOX4 inhibitor GKT137831 also delayed leukemic progression in FLT3-ITD xenograft mouse model. The FLT3-ITD-STAT5-NOX4-ROS-PTP/DEP1 axis may provide multiple targets for therapeutic inactivation in FLT3-ITD AML.

1.4.2 DSB repair is impaired in FLT3-ITD AML

In addition to an increase in DNA damage due to increased ROS level, FLT3-ITD might impair DDR directly. It has been reported that Ku70 and Ku86, key components of the classical NHEJ pathway, were decreased in FLT3-ITD AML [74]. On the other hand, DNA ligase IIIα (LIG3), a component of the MMEJ pathway, was increased. Therefore, FLT3-ITD signaling may affect the choice of DSB repair and skewed it from classical to alternative microhomology-based NHEJ. DSB repair via MMEJ resulted in larger DNA deletions and insertions than classical NHEJ. However, it still remains unclear on the effect of FLT3-ITD on error-free HR and the error-prone NHEJ.

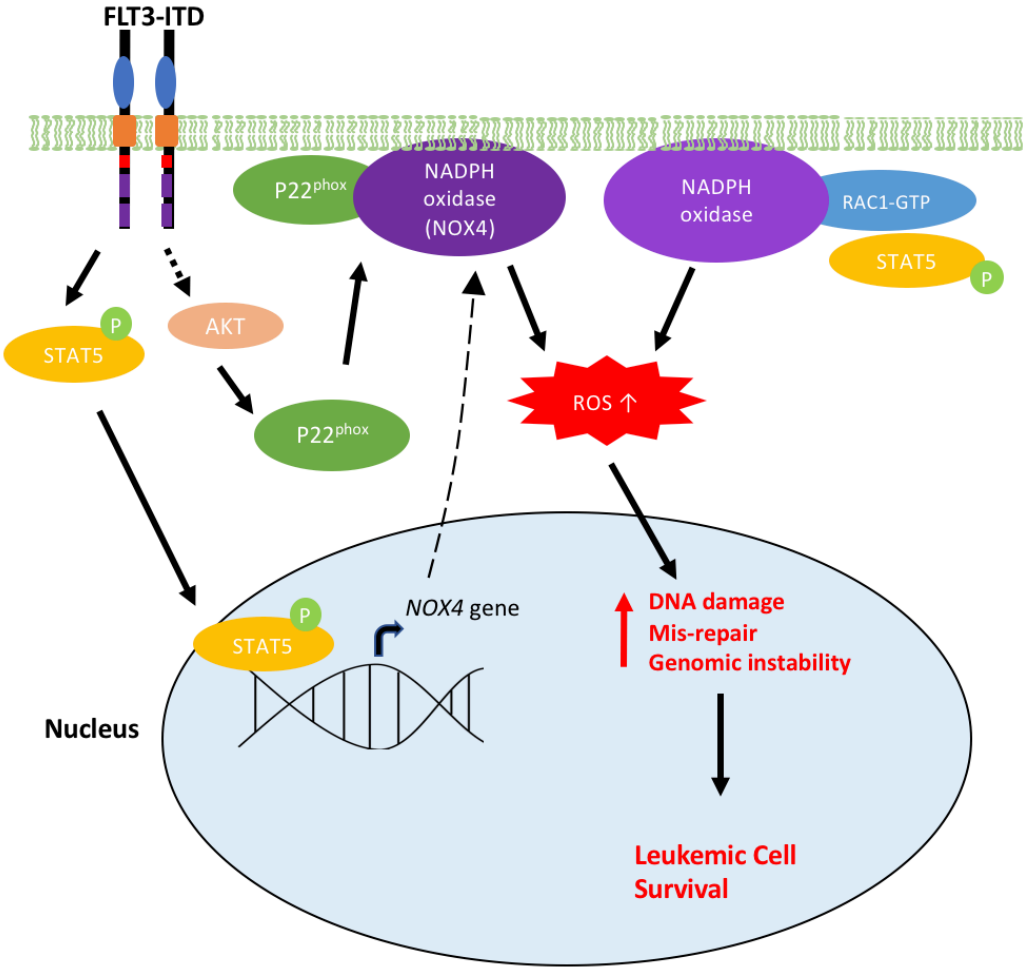

Figure 1.5 A schematic diagram showing the reported mechanism of elevated intracellular ROS via FLT3-ITD signaling.

FLT3-ITD signalling led to phosphorylation of STAT5. P-STAT5 subsequently translocated to nucleus and activated transcription of *NOX4*. P-STAT5 was also shown to keep RAC1 GTPase in its active GTP bound form. Active RAC1-GTP binding to NADPH complex was required for ROS production. FLT3-ITD signaling also stabilized $p22^{phox}$ protein via AKT signaling pathway and increased ROS production. The elevated ROS production in FLT3-ITD cells increased DNA damage and mis-repair and caused genomic instability. A low level of ROS was known to enhance leukemic cell survival.

1.4.3 Targeting DNA repair defect in FLT3-ITD AML

The DDR pathway has become a target for therapeutic intervention in human cancers, exemplified by the use of poly (ADP-ribose) polymerase (PARP) inhibitor in the treatment of *BRCA* mutant breast and ovarian cancers [75,76]. PARP detected and bound to DNA SSB breakpoint where it initiated synthesis of PAR chain to recruits other proteins involved in BER. PARP inhibition impaired BER and led to accumulation of SSB. Unrepaired SSB resulted in collapsed replication forks during DNA replication and hence the formation of DSB. In cancers with loss-of-function *BRCA1/2* mutation in which HR was defective, PARPi resulted in excess DSB that recruited error-prone NHEJ, causing genomic instability and apoptosis. The use of PARPi to induce synthetic lethality has been tested in clinical trials since 2003 [77]. And a decade later, PARP inhibitors Olaparib (2014) and rucaparib (2016) were FDA-approved to treat advanced, chemo-resistant ovarian cancer patients with germline *BRCA1/2* mutations. And later in 2017, niraparib was also approved for treatment of various solid tumours including primary peritoneal, ovarian, fallopian tube that are sensitive to platinum treatment [78,79]. Most importantly, AML carrying t(8;21) and t(15;17) showed down-regulation of DDR genes and defective DDR and they were extremely sensitive to PARPi [41]. The aforementioned DDR defects in FLT3-ITD AML and the resulting increase in PARP1-depedent MMEJ repair support the proposition that PARP may be a therapeutic target in this AML subtype.

Chapter 2. Study Objectives

Since its first description of FLT3-ITD in AML in 1996, much has been learnt about its prognostic significance, aberrant signaling and potential as a therapeutic target[80]. In particular, midostaurin was recently approved for treatment of newly diagnosed FLT3 mutant AML in combination of conventional chemotherapy and more potent and specific FLT3 inhibitors including quizartinib [81], gilteritinib [82] and crenolanib [83,84] have also been tested and reported in relapsed or refractory settings. However, disease relapse remains to be an important cause of treatment failure of FLT3 inhibitor-based regimen.

The cumulative evidence about increased ROS production, genomic damage and defective DSB repair in FLT3-ITD AML collectively supported the hypothesis that DDR defect may provide a new direction for therapeutic targeting. The works described in my Ph.D. thesis aimed to ask 3 important questions in this area of AML leukemogensis:

i. Is HR defective in FLT3-ITD AML and what is/are the mechanisms?

ii. Is PARP inhibitor effective in FLT3-ITD AML and how?

iii. What is/are the candidate genetic targets that can be exploited in the treatment of FLT3-ITD AML in combination with PARP inhibitors?

To address these questions, laboratory platforms have been developed both in HKU and KCL and the methodologies were described in the following sections.

Chapter 3 Materials and Methods

3.1 Primary sample processing

Bone marrow (BM) blood or peripheral blood (PB) collected from AML patients were stored at 4 ºC prior to processing. The samples were usually processed on the same day or no later than the next morning. Ficoll-Paque™ Plus solution was used to isolate the mononuclear cell (MNC) fraction rich in AML blasts by density-gradient centrifugation. The processed primary samples were cryopreserved in our liquid nitrogen biobank.

The standard operating procedure (SOP) for primary sample processing was as following: The whole blood (WB) sample was centrifuged at 1100 rpm for 10 minutes at room temperature to isolate the supernatant fraction. The plasma was purified by centrifuging the supernatant fraction at 3000 rpm at 4 ºC for 10 minutes to remove platelet or cell debris and stored at -80 ºC. The bottom fraction of WB, containing the buffy coat and red cells were diluted with Hanks' Balanced Salt Solution (HBSS) to final volume of 20 mL, carefully laid on 20 mL Ficoll-Paque™ Plus solution. The density-gradient centrifugation was performed at 1200 rpm for 30 minutes at room temperature (acceleration = 7, deceleration = 0). The middle layer, containing the MNC fraction was isolated by disposable Pasteur pipette and washed twice with 40 mL of HBSS. The cells were resuspended in HBSS and counted with a hematocytometer with 1:1 ratio of Trypan Blue (0.4% solution). For RNA work, 5 million cells were resuspended in 1 mL TRIzol (Life Tech) and stored at -80 ºC for subsequent RNA extraction. The remaining MNC were resuspended in pre-cooled freezing medium (10% dimethylsulfoxide (DMSO), 20% fetal bovine serum (FBS) and 70% HBSS) to final concentration of 20 to 40 million cells/ mL and cryopreserved

in Mr. Frosty™ freezing containers overnight at -80 ºC overnight prior to the transfer and long-term storage in liquid nitrogen tanks.

3.2 Culture and maintenance of cell lines

3.2.1 Human acute myeloid leukemia cell lines

Human leukemia cell lines (MOLM-13, MV-4-11 and NOMO-1) were originated from DSMZ and ATCC and maintained according to their protocols as listed in Appendix 1.

3.2.2 Ba/F3 cell line and its derivatives

Murine B lymphoid cell line, Ba/F3, and its derivatives transduced with *pLKO.1-blast* (Addgene #26655) carrying *FLT3-ITD* were generous gifts from Dr. Jerome Tamburini in the Institut Cochin, Université Paris Descartes, Paris, France. The cells were cultured in RPMI supplemented with 10% FBS and 1% P/S. Murine IL-3 cytokine (PeproTech) was added to the parental Ba/F3 line at final concentration of 2 ng/ mL but it was not required for the Ba/F3 FLT3-ITD line.

3.3 *In vitro* drug treatment

Ba/F3 parental and Ba/F3 FLT3-ITD cells were seeded in 96-well plate at 0.2 x 10^5 cells in 100 µL culture medium and treated with different drug concentrations for three days. On day 3, 10 µL PrestoBlue® cell viability reagent (Life Tech) was added into each well followed by 4 hours of incubation. The fluorescence signal of PrestoBlue® cell viability reagent was measured by FLUOstar OPTIMA microplate reader at 560 nm excitation and 590 nm emission.

Colony forming assay of murine *Flt3* $^{ITD/+}$ *x Npm1* $^{c/+}$ and *MLL-AF9* leukemic cells was carried out by plating 1-3 x10^3 cells in MethoCult^{TM} M3234 (Stemcell Technology) supplemented with murine cytokines: 20 ng/mL SCF, 10 ng/mL IL-3, 10 ng/mL IL-6 and 10 ng/mL (PeproTech) together with inhibitors at stated concentration. The number of colonies was scored after 7 days.

3.4 RNA extraction and reverse transcription polymerase chain reaction

3.4.1 RNA extraction

The primary MNC was resuspended in 1 mL TRIzol (Chapter 3.1) and was homogenized in a 1mL 29-gauge syringe. The cell lysate was incubated for 5 minutes at room temperature. Then, 200 µl of chloroform was added to the tube and incubated for 5 minutes at room temperature. The sample was then separated into aqueous, interphase and organic phase by centrifugation at 13,400 x g for 15 minutes at 4°C. The upper aqueous phase containing RNA was transferred to a new sterile 1.5 ml microcentrifuge tube, while the interphase (DNA) and lower organic phase (proteins) were discarded. To precipitate the RNA, 500 µl of isopropanol was added and incubated at room temperature. RNA pellet was collected by centrifugation at 13,400 x g for 10 minutes at 4°C, washed with 1 ml of 75% (v/v) ethanol, centrifuged at 13,400 x g for 5 minutes at 4°C, air-dried for 10 minutes and dissolved in 20 µl of DEPC-treated water. Purity and quantity of total RNA were determined by the absorbance ratio of 260 nm/280 nm (protein impurity) and 260 nm/230 nm (organic solvent impurity) by Thermo Scientific NanoDrop 2000 Spectrophotometer, of which most of RNA samples had both ratio greater than 1.8.

3.4.2 Reverse transcription polymerase chain reaction

Extracted RNA was reversed-transcribed to first strand complementary DNA (cDNA) using SuperScript II reverse transcriptase kit (Thermo Fisher Scientific). Of note, 1 μg of RNA was used for input and 1 μl of random primers (50 ng/ mL) was used for amplification. The cDNA was stored at -80 °C until use.

3.5 Real-time quantitative PCR (RT-QPCR)

The cDNA synthesized in chapter 3.4.2 was diluted 5-fold with RNase-free water as template for RT-QPCR using the SYBR Green Select Master Mix (Thermo Fisher Scientific) and StepOnePlus Real-Time PCR System (Applied Biosystems). The list of primers used for RT-QPCR is listed in Appendix 2. Relative quantification of the gene expression was calculated by the comparative algorithm (ΔCt) using β-actin as internal control [85]. Comparison of relative gene expression was normalized to ΔCt control group. The relative gene expression was calculated as

$2^{-\Delta\Delta Ct} = 2^{-(\Delta Ct\ target\ -\ \Delta Ct\ control)}$.

3.6 Western Blot

Cell pellet was lysed with CelLytic™ MT Cell Lysis Reagent (Sigma) with addition of protease and phosphatase inhibitors cocktail (Thermo Scientific) to extract soluble protein fraction. The extracted protein was mixed with Laemmli loading dye and denatured at 95°C for 5 min, separated by sodium dodecyl sulfate polyacrylamide gel electrophoresis (SDS-PAGE) (7.5, 10 or 12%) and was transferred to 0.2 μm nitrocellulose membrane. The blot was then incubated with blocking buffer (5% non-fat milk in PBST) for 30 mins and probed with primary antibody overnight

at 4°C and secondary antibody at room temperature for 1 hour. Primary and secondary antibodies used are listed in Appendix 3. The ECL signal was developed with Luminate Forte Western HRP substrate (Millipore) and detected using the ChemiDoc MP Imaging System (Bio-Rad).

3.7 Immunofluorescence Microscopy

At the experimental endpoint, the cells were washed once with 1X PBS and resuspended at 1 million/ mL. 100 µL of the cells were cytospun onto glass slides at 400 g for 5 mins and then fixed with 4% PFA for 15 mins and blocked with 0.5 % Triton X-100, 1% BSA in PBS for 30 minutes. The slides were then incubated at 4°C overnight with mouse anti- γ-H2AX (ser139) (Upstate clone JBW301 #05-636) at 1:200 dilution overnight. The slides were then washed 3 times with 0.5% Triton X-100 in PBS and subsequently incubated with 1:200 goat anti-Mouse IgG Alexa Fluor 488 (ThermoFisher) at room temperature in dark for 1 hour. The slides were then washed 3 times with PBS and mounted with coverslips using fluorescence mounting medium (Dako).

Fluorescent images were taken with Olympus IX70 (Olympus) using 20X/0.3 NA objective and acquired by Olympus DP71 (Olympus) and Olympus DP-BSW basic Software.

3.8 Neutral comet assay

Comet assay was performed using CometAssay® kit (Trevigen) according to the manufacturer's neutral comet assay protocol. The comet images were captured using fluorescent microscope (Leica) were analysed using OpenComet [86].

3.9 General flow cytometry experiments

All flow cytometry (FACS) were performed with LSRII Fortessa Analyzer (BD Biosciences) or FC500 (Beckman Coulter), and data was analyzed using FlowJo 7.6.1 software (Tree Star, Inc.).

3.9.1 Intracellular reactive oxidative species (ROS) level measurement

Intracellular ROS was measured using the general oxidative stress indicator CM-H2DCFDA dye. This dye was cell permeable and was retained in living cells. The subsequent oxidation of CM-H2DCFDA in cells yielded a fluorescent adduct that was quantified by flow cytometry using the FITC (FL-1) channel.

The CM-H2DCFDA was freshly reconstituted in DMSO at 10 mM immediately before each experiment and all the experimental procedure must be kept in dark at all time prior to FACS analysis.

At experimental endpoint, cells were washed once with pre-warmed PBS and then incubated with 10 μM of the probe in PBS at 37 ^{o}C for 30 minutes. The probe was then washed off with PBS and incubated again at 37 ^{o}C for 30 minutes to recover and to ensure the oxidation reaction was completed prior to flow cytometry.

3.9.2 Immunophenotypic analysis of primary murine cells

The leukemic mice were first euthanized using CO_2 chamber. Total bone marrow cells were harvested from femurs and tibias, spleen and liver cells were homogenized and filtered with 0.45 μm cell strainer. Red cells were lysed by BD Pharm Lyse^{TM} for 5 minutes on ice in dark and washed with PBS with 2% FBS. The cells were stained

with mouse-specific PE/Cy7 anti-CD11b (Mac-1, clone M1/70), PerCp/Cy5.5 anti-Gr1 (clone RB6-8C5), PE anti-c-Kit (clone 2B8), FITC anti-CD45.1 (clone A20) and APC anti-CD45.2 (clone 104) antibodies from BioLegend. All antibodies are used at a dilution of 1:200 at 4 °C for 30 mins and analysed by BD LSRII flow cytometer (BD Biosciences).

3.10 Lentivirus packaging

HEK293FT cells were used for packaging of lentivirus. The cells were seeded at 50% confluent overnight in 100 mm dish. The next day, 4 μg of the lentiviral packaging plasmid *pCMV-dR8.91*, 4 μg of the envelop plasmid *pMD2.G* and 7 μg of the transfer plasmid were co-transfected using 30 μl of lipofectamine 2000 (Life tech) per 100 mm dish. At 8-hour post-transfection, the dishes were replaced with fresh complete DMEM medium. 48 hours later, the supernatant was harvested and filtered through a 0.45 μm filter. The viral particles were concentrated 20-fold by ultracentrifugation at 25,000 x g for 2 hours at 4 ^{o}C. The concentrated lentivirus was aliquoted and stored at -80 ^{o}C.

3.11 Traffic Light Reporter (TLR) assay

The TLR assay was developed by Certo *et al* in 2011 [87]. The assay consisted of 2 separate plasmids: *pCVL Traffic Light Reporter 1.1* (Addgene #31482) and *pCVL SFFV d14GFP EF1s HA.NLS.Sce* (Addgene #31476), in which both plasmids were packaged separately in lentivirus.

The cells were first transduced lentivirally with the TLR plasmids and the next day puromycin was added at final concentration of 1 μg/ mL for selection of plasmid containing clones for additional 2 days. The cells were then washed with PBS and

transduced with *pCVL SFFV d14GFP EF1s HA.NLS.Sc*e lentivirus which expressed the I-SceI endonuclease and contained the GFP donor template. Two days post transduction, the cells were analysed by FACS.

3.12 DNA damage response (DDR) *shRNA* library screening

The cloning protocol of *shRNA* library, the *shRNA* hairpin sequences with improved knockdown efficiency and Miseq library preparation protocol were provided by Dr. Johannes Zuber's group [88]. A brief procedure is described as below.

3.12.1 Cloning of DDR shRNA library plasmids

The DDR *shRNA* library consisted of all reported genes with functions annotated to DNA damage response pathways from published databases KEGG and REPAIRtoire, and review papers [89,90]. Multiple *shRNA* libraries were ordered from Agilent (United States) and each gene had 5 unique *shRNA* hairpins. The mouse DDR *shRNA* library was amplified by library-specific PCR primers with low PCR cycles and cloned into lentiviral vector *pRRL-GFP-Puro*. To ensure complete representation of the hairpin library pool, the target number of bacterial colonies was at least 100-fold the total number of hairpins. In the case of mouse DDR library with ~1,200 unique hairpins, at least 120,000 single colonies were transformed. All colonies were recovered in LB broth overnight and plasmid DNA was extracted by Gigaprep (Qiagen).

3.12.2 Experimental Scheme of DDR shRNA library screening

Mouse DDR *shRNA* library was packaged into lentivirus and the virus was titrated such that less than 30% GFP+ cells post transduction, to ensure that MOI was around

1. Twenty million of *Flt3* $^{ITD/+}$ *x Npm1* $^{c/+}$ leukemic cells were transduced with mouse DDR *shRNA* lentivirus for 2 days. GFP+ cells were sorted using BD FACSAria cell sorter. 1 x 10^5 sorted cells were transplanted into sub-lethally irradiated (500 Rads x 2 doses) CD45.1 SJL mice by intravenous injection. Two weeks post-transplantation, the experimental mice were divided into two groups and treated with either 50mg/kg Olaparib or vehicle control by intraperitoneal injection 5 days per week for 2 weeks. After 4 additional weeks, the mice were euthanized. Total bone marrow cells were harvested from femurs and tibias.

3.12.3 Preparation of sequencing library for MiSeq

Genomic DNA was extracted from cell pellet using QIAamp DNA Mini Kit (Qiagen). To keep 1000-fold representation of a pool of 1,200 *shRNA* at MOI= 1, the total amount of DNA input for PCR is 7 μg DNA, assuming 1ng genomic DNA contained the DNA from 167 diploid cells. Using PCR primers containing the P5 and P7 adaptor sequences and unique barcodes for the Illumina platform, individual DNA samples were amplified and barcoded. The purified DNA samples were quantified by Qubit and pooled together at 6 nM final concentration. The final DNA samples were sequenced using single-read Miseq V2 50 cycle kit (Illumina) with custom sequencing primer at READ1 position.

3.12.4 Bioinformatics analysis

Ms. Claire Lynn, PhD student from Prof. Eric So's lab in Kings College London performed the majority of the bioinformatics analysis, including the processing of the raw sequencing data, demultiplexing of sequencing reads, mapping of reads to unique

hairpins and the statistical analysis. I performed the final analysis and data interpretation.

3.13 *In vivo* drug treatment of Olaparib and chemotherapy drugs in MOLM-13 xenograft model

8-10 weeks old *NOD/SCID/IL2Rg*$^{-/-}$ (NSG) mice were sub-lethally irradiated with 250 cGy 4 hours before transplantation. 1 x 10^5 of MOLM-13 cells with luciferase reporter were resuspended in 150 µL PBS and transplanted into NSG by intravenous injection using 29 G syringe. At 4-day post-transplantation, experimental mice were injected with 150 mg/kg D-luciferin substrate intraperitoneally and bioluminescence imaging were acquired with PE IVIS Spectrum *in vivo* imaging system (PerkinElmer). The dosage and drug delivery method that mimicked the patient "7+3" regimen was based on Wunderlich *et al* [91], which comprised 5 days of cytarabine (25mg/kg) by intraperitoneal injection and doxorubicin (1.5mg/kg) by intravenous injection on day1-3. Olaparib (25mg/kg) was administrated by intraperitoneal injection for 5 days. Post-treatment bioluminescence was taken on the 11th day post-transplantation.

3.14 Statistical analysis

Unless otherwise specified, data were expressed as means ± standard error of the mean (SEM). Comparisons between groups of numerical data were evaluated using Student's t-test. P-values < 0.05, < 0.01 and < 0.001 were considered statistically significant, and were represented with asterisk (*), (**) or (***). Survival analysis of mouse experiments was performed using the Kaplan-Meier method. Differences in survival were determined using log-rank test. Sample size (N) and replicates (n) of all experiments were indicated in their corresponding figure legends.

Chapter 4. Homologous recombination in FLT3-ITD AML was affected with possible mechanistic linkage to down-regulation of *BRCA2.*

4.1 Introduction

FLT3 is one of the most common mutations in AML [1]. Its molecular structure has been described in Chapter 1. The JM domain negatively regulates FLT3 function by inhibiting phosphorylation. ITD commonly occurs in JM domain, thereby disrupting the auto-regulatory function and giving rise to constitutive activation of FLT3 and its downstream signaling pathways such as AKT, ERK and STAT5 [57]. Emerging evidences show that FLT3-ITD AML is associated with increased ROS production and DNA damage. At the same time, DDR may be defective [70,72,74,92,93] but the mechanistic link with particular reference to the relative contribution of HR and NHEJ is presently unclear.

4.2 Down-regulation of *BRCA2* in FLT3-ITD primary AML samples

To investigate the link between FLT3-ITD AML and DDR, expression of critical DDR genes in primary AML samples was examined by quantitative real-time PCR. The study was restricted to *de novo* and cytogenetically normal AML at diagnosis to avoid changes in gene expression secondary to prior chemotherapy. To reduce variation in samples, only BM samples were used and all of them showed blast population ≥ 70%. A total of 18 FLT3-WT and 13 FLT3-ITD samples were recruited. Six apheresis samples from healthy donors who donated peripheral blood stem cell (PBSC) were included as control.

A panel of genes associated with apical kinase *ATM*, *ATR* and *DNA-PKcs*; DNA damage mediators *BRCA1*, *BRCA2* and *PARP1*; downstream response kinase *CHEK1* and *CHEK2* and effectors *TP53,* were examined. *BRCA2* expression was significantly down-regulated in FLT3-ITD AML. Those of *ATR* and *P53* were also down-regulated, albeit statistically significant (Fig. 4.1). Down-regulation of *BRCA2* in FLT3-ITD AML was further validated in a microarray database GSE15434 from a multicenter study investigating gene expression profiles of normal karyotype AML (WT=148; ITD=86) (Fig. 4.2) [94].

4.3 FLT3-ITD signaling was responsible for the suppression of *BRCA2* expression

The mechanistic link between FLT3-ITD and DDR genes with particular reference to *BRCA2* was evaluated in human FLT3-ITD+ AML cell lines MOLM-13 and MV-4-11 that carried *MLL-AF9* and *MLL-AF4* fusions respectively. NOMO-1 cell line that similarly harbored *MLL* translocation but wild-type *FLT3* was included as control. *BRCA2* expression was significantly reduced in MOLM-13 and MV-4-11 compared with that in NOMO-1, consistent with the observations made in primary samples (Fig. 4.3).

To ascertain if *BRCA2* downregulation was secondary to FLT3-ITD signaling, gene expression was examined after treating the 3 cell lines with a FLT3-specific inhibitor quizartinib. At a dose up to 5 nM that had been shown to suppress FLT3 signaling in MOLM-13 and MV4-11, *BRCA2* expression was significantly increased [95]. However, there was no significant effect in NOMO-1 (Fig. 4.4).

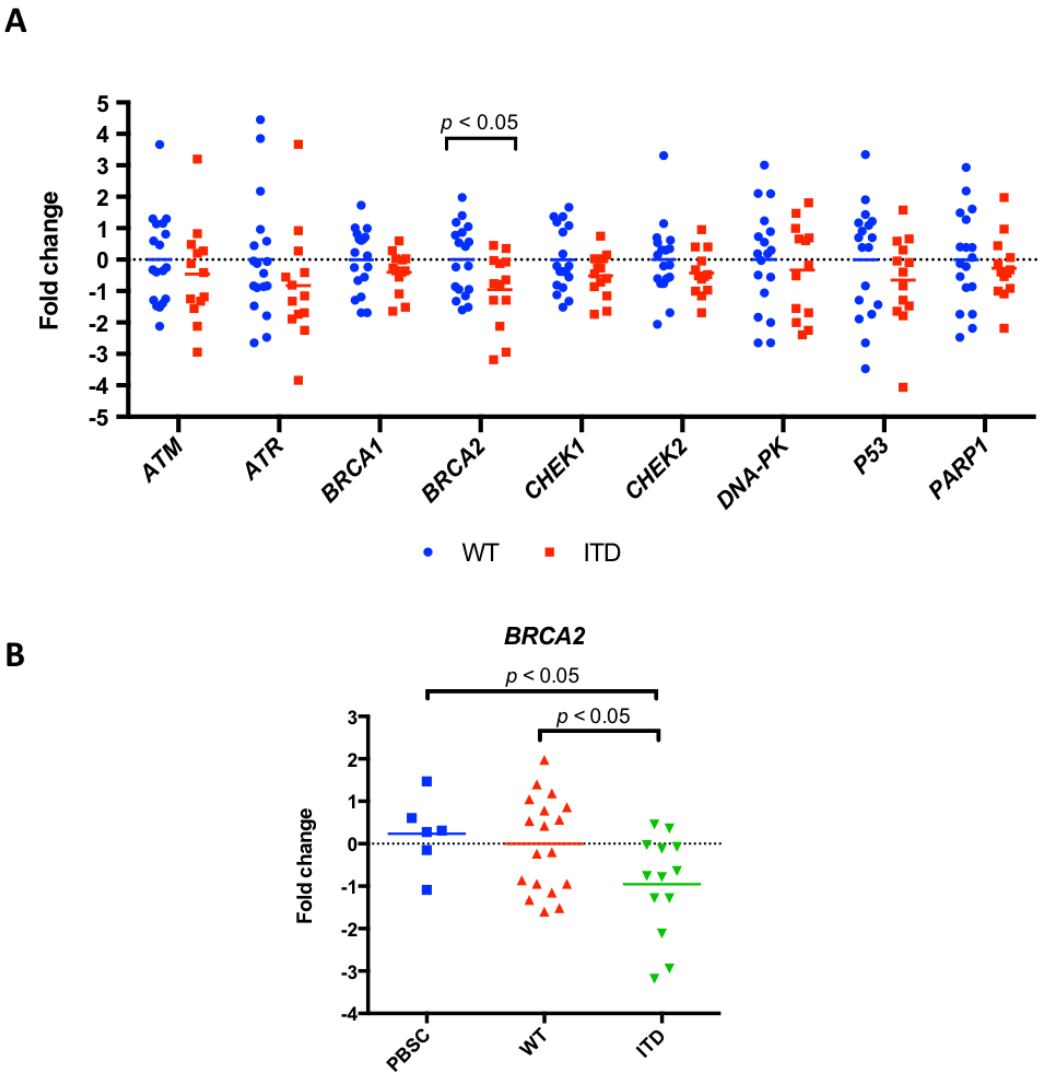

Figure 4.1 Gene expression profile of DNA repair genes in primary AML patients.

(A) Quantitative Real Time PCR was performed using complementary DNA (cDNA) of leukemic myeloblasts from bone marrow of normal karyotype AML patients. Wild-type FLT3 (WT): N=18; FLT3-ITD (ITD): N=13. **(B)** Among all DNA repair genes tested, only *BRCA2* was significantly down-regulated when compared to normal PBSC control (N=6) and also wild-type FLT3 AML samples.

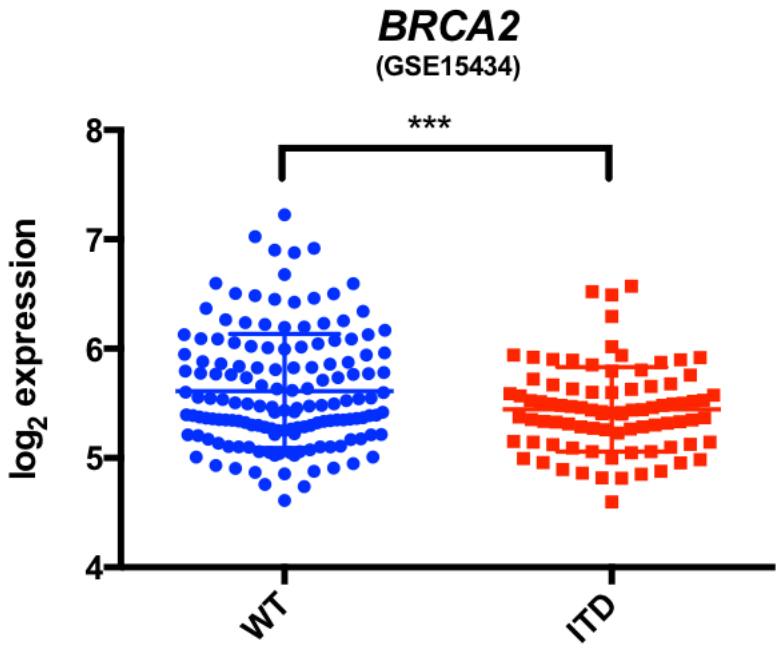

Figure 4.2 *BRCA2* expression profile from GSE15434.

All the samples in this study were normal karyotype AML samples obtained from untreated patients at the time of diagnosis. Purified mononuclear cells were collected for microarray analysis. Samples were collected from Dresden, Munich and Ulm. The data was downloaded from Gene Expression Omnibus under the accession GSE15434. The 214727_at probe was used to hybridize and quantity expression of *BRCA2.* Wild-type FLT3 (WT): N=148; FLT3-ITD (ITD): N=86. p-value < 0.001.

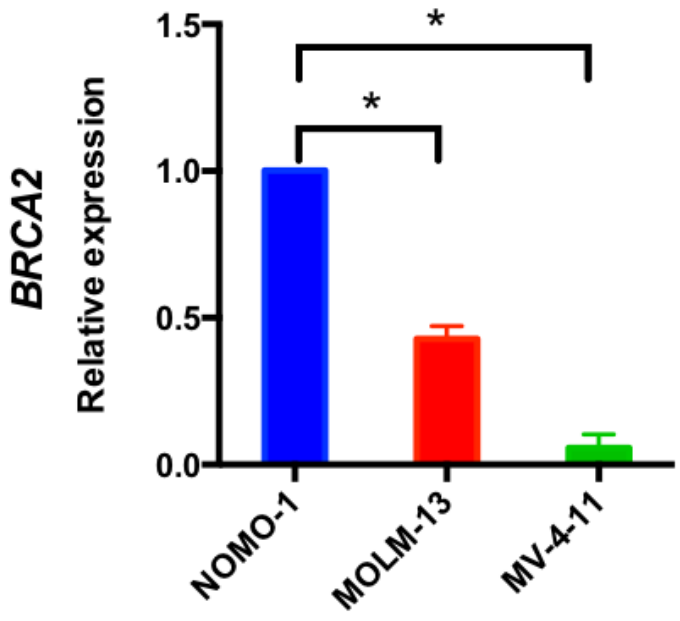

Figure 4.3 *BRCA2* expression of human AML cell lines.

Quantitative Real Time PCR was performed using cDNA of human AML cell lines. All the cells here harbored *MLL-fusion* mutations: NOMO1 (*MLL-AF9*); MOLM-13 (*MLL-AF9*); and MV-4-11 (*MLL-AF4*) respectively. NOMO1 with wild-type FLT3 serves as the control cell lines. MOLM-13 was heterozygous for FLT3-ITD mutations whereas MV-4-11 was homozygous for FLT3-ITD. n=2; * $p < 0.05$.

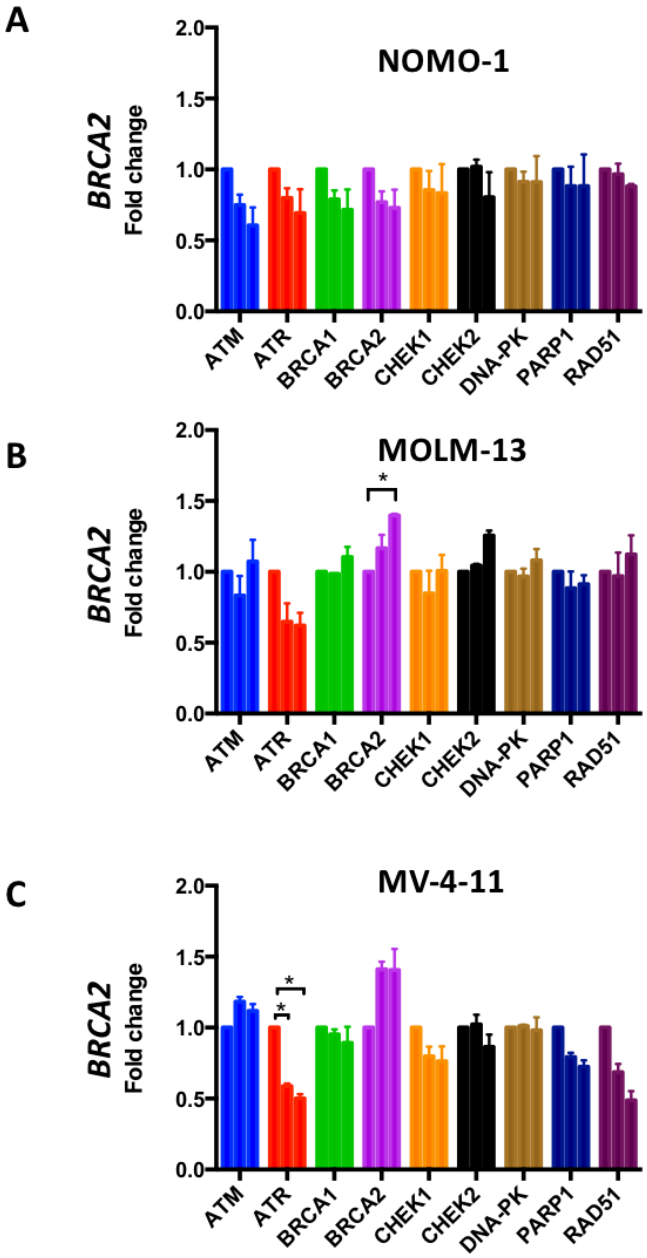

Figure 4.4 Gene expression profile of DNA repair genes in human AML cell lines after treatment of FLT3 inhibitor, quizartinib.

(A) NOMO-1, **(B)** MOLM-13 and **(C)** MV-4-11 AML cell lines were treated with 0, 1 and 5 nM of quizartinib for 4 hours. Relative gene expression was quantified by QPCR and normalized to vehicle control. Increase in *BRCA2* was observed in FLT3-ITD AML cell line MOLM-13 and MV-4-11 after quizartinib treatment but not in FLT3-WT NOMO-1 control. n=2. * $p<0.05$.

To more clearly define the link between FLT3-ITD signaling and DDR, an isogenic Ba/F3 FLT3-ITD cell model was used in which Ba/F3 FLT3-ITD cells survived on autonomous FLT3-ITD signaling while parental Ba/F3 cells survived on IL3 that was supplemented in culture medium. Consistent with the observations in primary AML samples and cell lines, murine *Brca2* was significantly down-regulated in Ba/F3 FLT3-ITD line (Fig. 4.5A) and quizartinib induced a significant increase in these cells (Fig. 4.5B).

4.4 Homologous recombination activity was decreased in FLT3-ITD cells

Effective DDR is critical for the maintenance of genomic integrity in cells that are exposed to genotoxic agent [96,97]. Without timely repair, DNA breaks can cause genomic instability and cell death. DSB repair is accomplished by error-free HR that utilizes the sister chromatin as a template for DSB repairs and is dependent on intact BRCA2 protein that regulates the intracellular location and DNA binding of RAD51 [98-100]. Loss-of-function *BRCA2* mutation resulted in defective DSB repair and predisposes patients to breast or ovarian cancers [101,102]. Therefore, the observations of *BRCA2* down-regulation in FLT3-ITD+ AML supported the proposition that DDR may be defective in this AML subtype and it was tested in subsequent experiments.

The Traffic Light Reporter (TLR) assay was used to evaluate the efficiency and repair fidelity of DSB in Ba/F3 FLT3-ITD line [87], which allowed a direct measurement of the relative efficiency of error-free homologous recombination (HR) and error-prone non-homologous end-joining (NHEJ) at a particular DSB site induced by

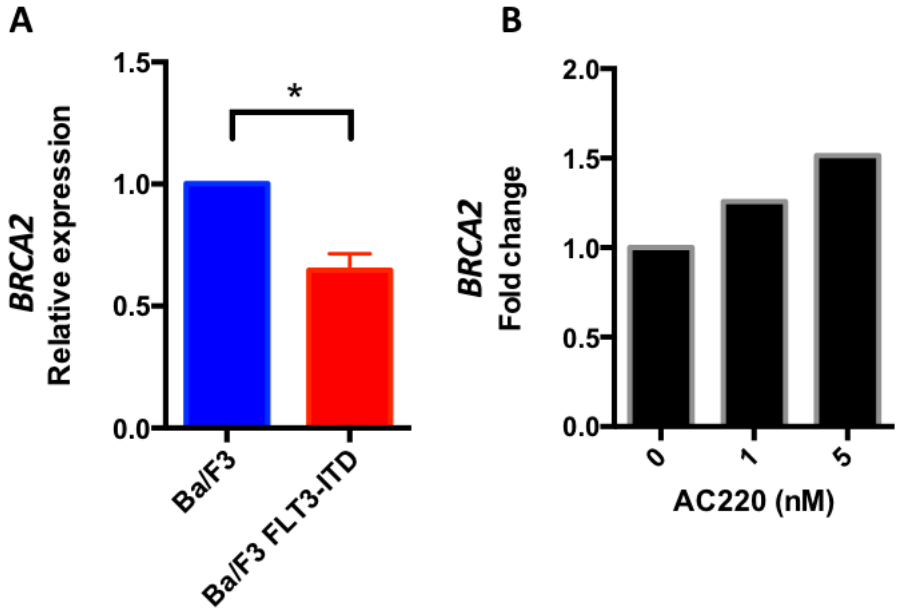

Figure 4.5 *Brca2* expression in Ba/F3 FLT3-ITD isogenic model.

Murine pro-B cell line was lentivirally transduced with coding sequence of human *FLT3-ITD*. **(A)** QPCR result of *Brca2* transcript level shows down-regulation of *Brca2* in Ba/F3 FLT3-ITD line when compares to parental control. n=3; $p<0.05$. **(B)** Inhibition of FLT3-ITD signaling with AC220 results in rescue of *Brca2* expression in Ba/F3 FLT3-ITD line by QPCR. n=1.

endonuclease. The mutant *GFP* (containing a premature termination codon, *ΔGFP*) and *mCherry* open reading frame (ORF) in the TLR were fused by a ribosome skipping sequence (*T2A*) that allowed translation of 2 distinct polypeptides without forming a peptide bond. *GFP* and *mCherry* ORF were positioned in different frames and DSB was induced at a unique recognition site for endonuclease I-SceI in the mutant *GFP* ORF. If NHEJ repair had occurred, it would place *ΔGFP* in frame with *mCherry* in 1 out of 3 events, leading to mCherry fluorescence. If HR repair had occurred, the *GFP* donor template that was lentivirally transduced after TLR would replace *ΔGFP* in TLR, leading to GFP fluorescence (Fig. 4.6). Compared with the parental line control, DSB repair by HR was significantly decreased in Ba/F3 FLT3-ITD while DSB repair by NHEJ was not significantly different (Fig. 4.7 & 4.8). In summary, the data demonstrated that FLT3-ITD down-regulated *BRCA2*, impaired HR and DSB repair fidelity in FLT3-ITD AML.

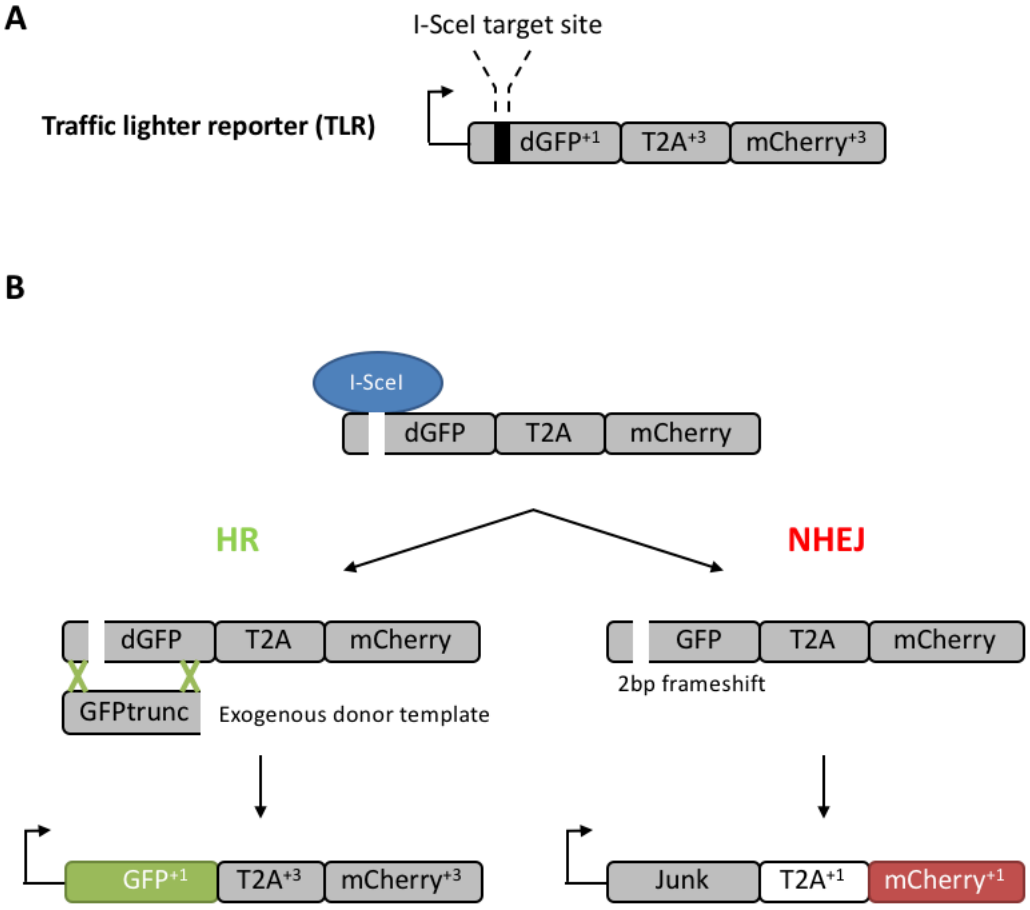

Figure 4.6 Principle of the Traffic Light Reporter (TLR) assay.

(A) The simplified vector map of the TLR plasmid illustrating the structure of the TLR transcript. The open reading frame relative to the initial defective GFP (dGFP) was indicated in superscript. **(B)** I-SceI nuclease cleaved the TLR at the target site and induced double-stranded break (DSB). The DSB could be either repaired via the homology-directed recombination using the exogenous donor template and reconstituted the full GFP sequence and the cells would emit green fluorescence. If the DSB underwent non-homologous end joining (NHEJ), one in third chance would result in 2bp frameshift and translated an in-frame mCherry protein and emitted red fluorescence. The diagram was adopted from the original TLR paper [87].

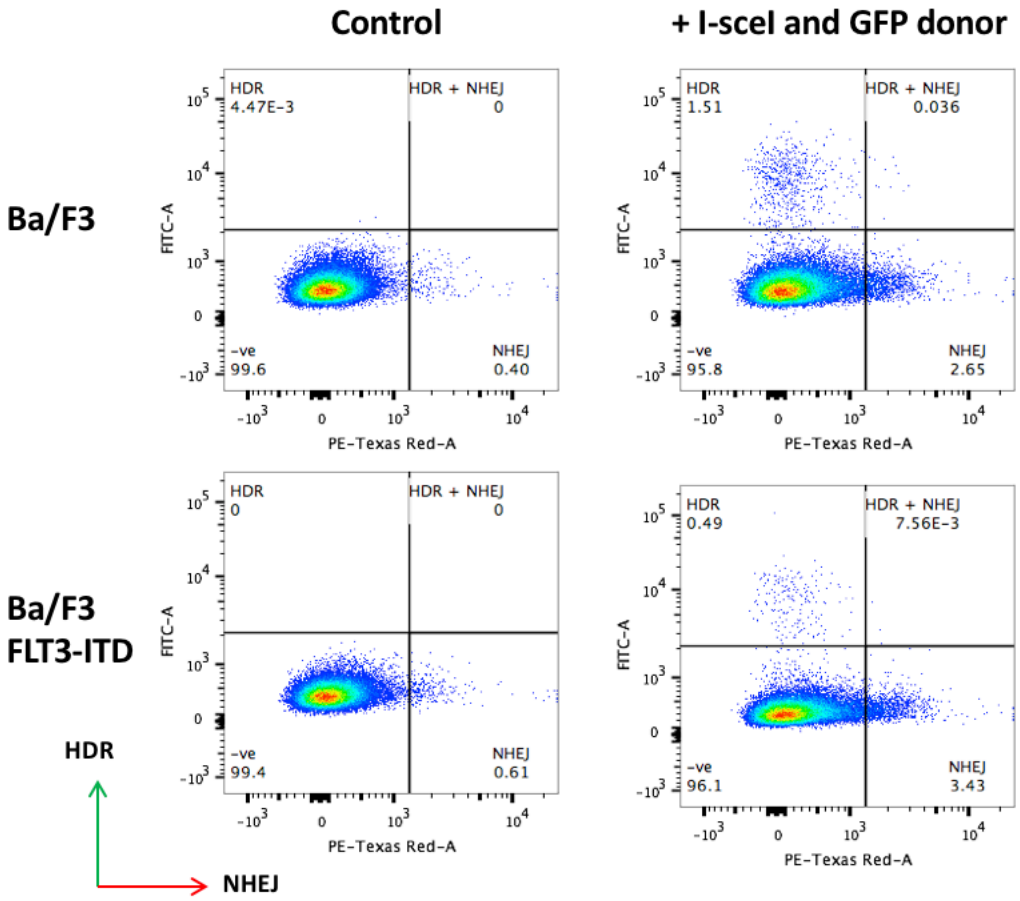

Figure 4.7 Representative flow plot of the TLR reporter assay.

The Ba/F3 parental and FLT3-ITD cells stably expressing the TLR reporter construct were lentivirally transduced with a plasmid expressing I-SceI and GFP donor template. The transduced cells were analyzed by flow cytometer 2 days post transduction. Top left quadrat gated on GFP+ cells: cells underwent HR and bottom right quadrat gated on mCherry+ cells: those underwent NHEJ.

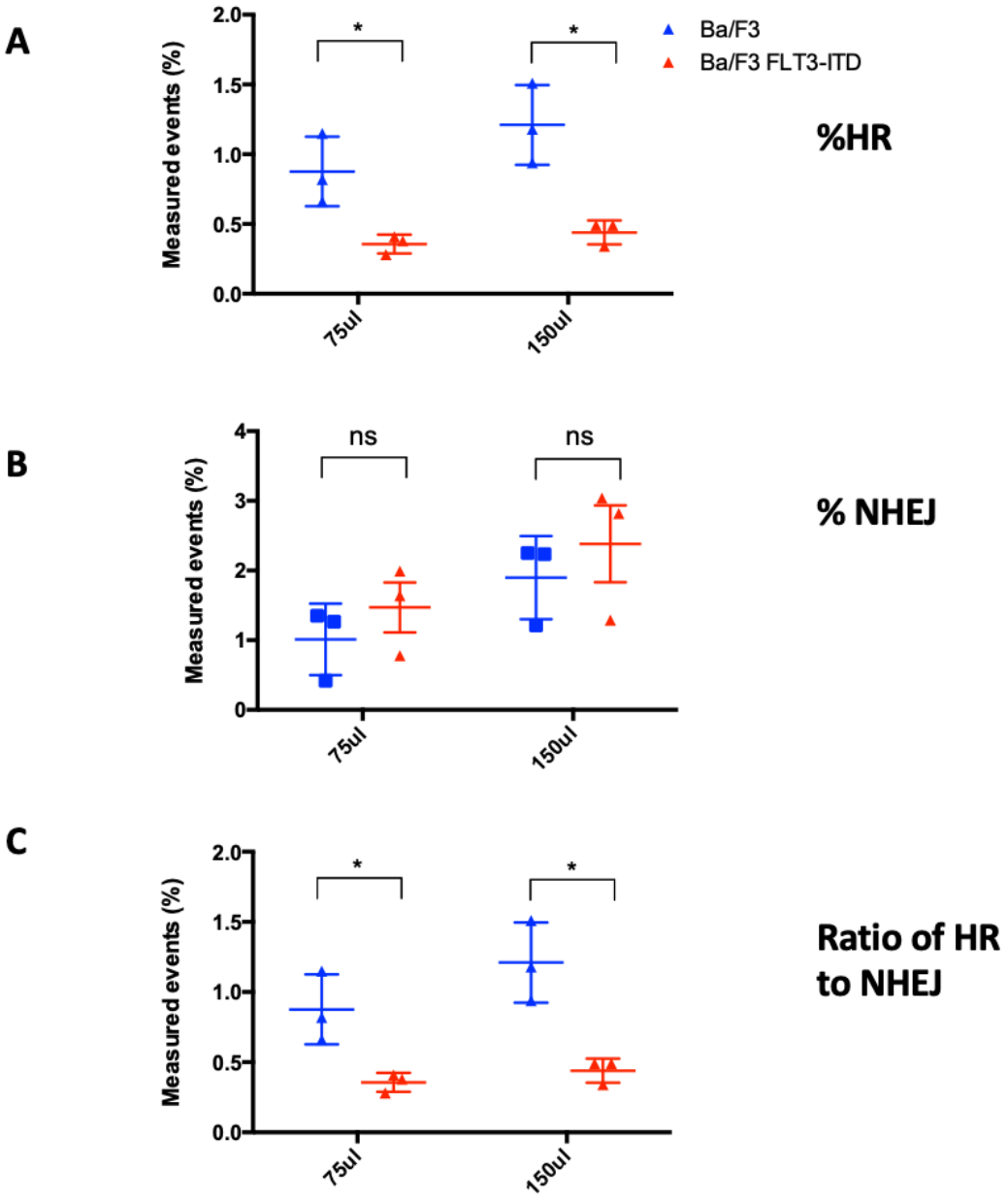

Figure 4.8 Statistical analysis of the TLR assay.

(**A**) & (**B**) Quantification of % measured events of GFP+ cells (HR) and mCherry+ cells (NHEJ) respectively. (**C**) Ratio of HR to NHEJ, representing the relative DSB repair fidelity. n=3. Error bar=SEM; *p*-value: * <0.05; *** < 0.001; ns: not significant.

Chapter 5. Targeting FLT3-ITD AML with PARP inhibitor

5.1 Introduction

Defective DDR plays an important role in the pathogenesis of AML [18]. Myeloblasts from FLT3-ITD+ AML patients showed a significantly higher level of reactive oxidative species (ROS) than AML patients with *FLT3* wild type alleles (FLT3-WT) [93]. Elevated level of both cytoplasmic and nuclear reactive oxidative stress (ROS) were observed in FLT3-ITD AML cell lines as well as murine cell line transduced with *FLT3-ITD* constructs [71,73,103,104]. In particular, decreased NHEJ and increased PARP1-dependent MMEJ activity resulted in large DNA insertions and deletions[74]. The data from Chapter 3 showed that FLT3-ITD+ cells had *BRCA2* down-regulation and reduced HR activity, this chapter examined whether drugs targeting DNA repair pathways, in particular, PARPi, could be used to intervene the leukemic development of FLT3-ITD transformed Ba/F3 cells.

5.2 PARP inhibitors selectively targeted FLT3-ITD AML *in vitro* by cell proliferation assay

To target key components in DDR, FLT3-ITD AML was treated with a panel of small molecular inhibitors targeting ATM, ATR, CHEK1/2 and PARP. Effects on leukemia growth *in vitro* were evaluated by Presto Blue colourimetric assay up to maximum plasma concentration reported in patients. Of the 4 inhibitors tested, PARP inhibitor Olaparib showed preferential inhibitory effects on Ba/F3 FLT3-ITD over the parental. ATM inhibitor KU-55933 also showed a modest but significant preferential effect on Ba/F3 FLT3-ITD (Fig. 5.1)

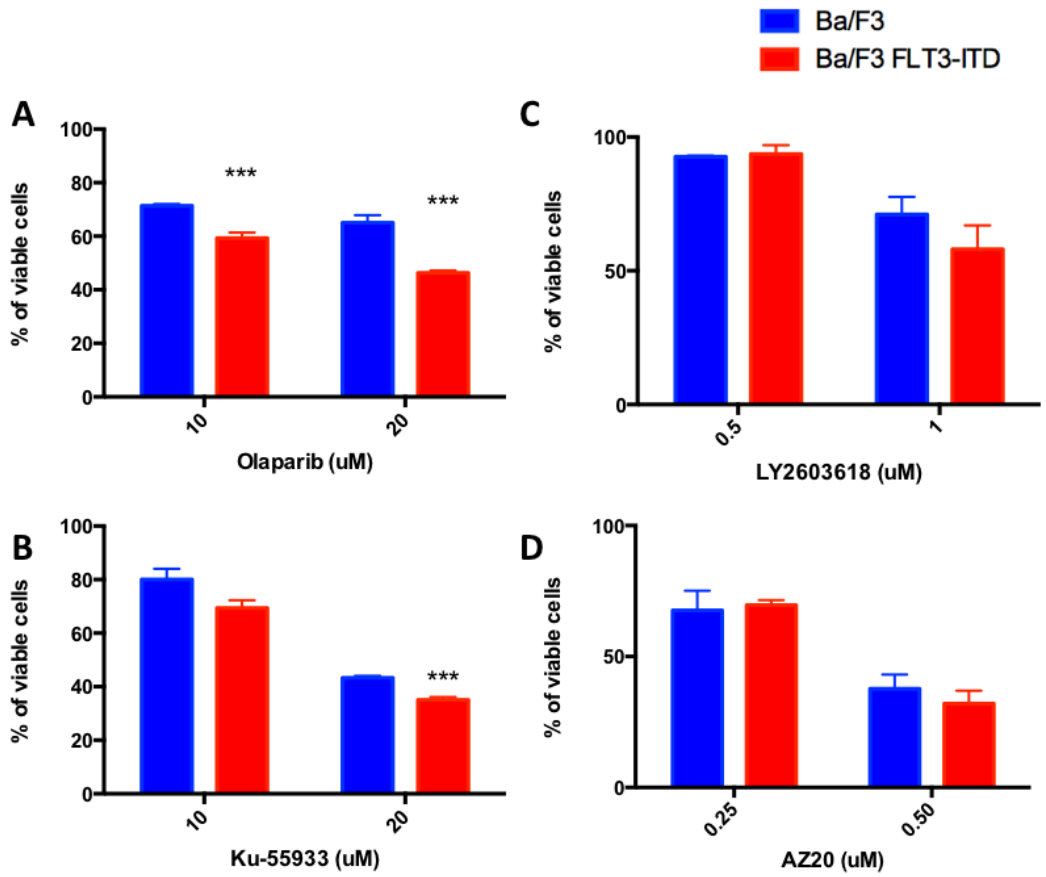

Figure 5.1 Cell proliferation assay of inhibitors targeting DNA repair proteins. Ba/F3 FLT3-ITD cells and the parental control line were treated with inhibitors for 3 days. The number of viable cells was measured by cell viability dye Presto Blue relative to the vehicle control. The inhibitors targeted **(A)** PARP; Olaparib, **(B)** ATM; Ku-55933, **(C)** CHEK1; LY2603618, and **(D)** ATR; AZ20. n=3; *** $p < 0.001$.

5.3 FLT3-ITD cells showed higher basal level of double-stranded DNA breaks that was accentuated by Olaparib.

In this section, the genotoxic effect of PARP inhibition in FLT3-ITD cells was examined, predicating on the premise that PARPi should impair SSB repair and cause DSB accumulation, driving FLT3-ITD cells to NHEJ pathway for DDR as *BRCA2* expression and HR activity were suppressed in this AML subtype. The error-prone NHEJ might induce genomic instability and apoptosis.

Gamma-H2AX (γ-H2AX) is a biomarker for DNA double-stranded breaks, of which DSBs in the chromatin initiate the phosphorylation of the histone H2AX at serine 139 [25]. By immunoblot analysis and immunofluorescence, basal level of γ–H2AX was higher in Ba/F3 FLT3-ITD cells when compared to control (Fig. 5.2), indicating a higher level of basal DSB. Olaparib treatment significantly accentuated DSB as demonstrated by an increase in γH2AX immunostaining.

The neutral comet assay, a single cell gel electrophoresis assay to detect genomic DSB for single cell, was performed to directly quantify the genomic DNA damage caused by FLT3-ITD oncogenic protein and the effects of Olaparib (Fig. 5.4A). The comet assay images were analysed by OpenComet (Fig. 5.4B) [86]. FLT3-ITD induced higher level of DNA DSB which was accentuated by Olaparib treatment.

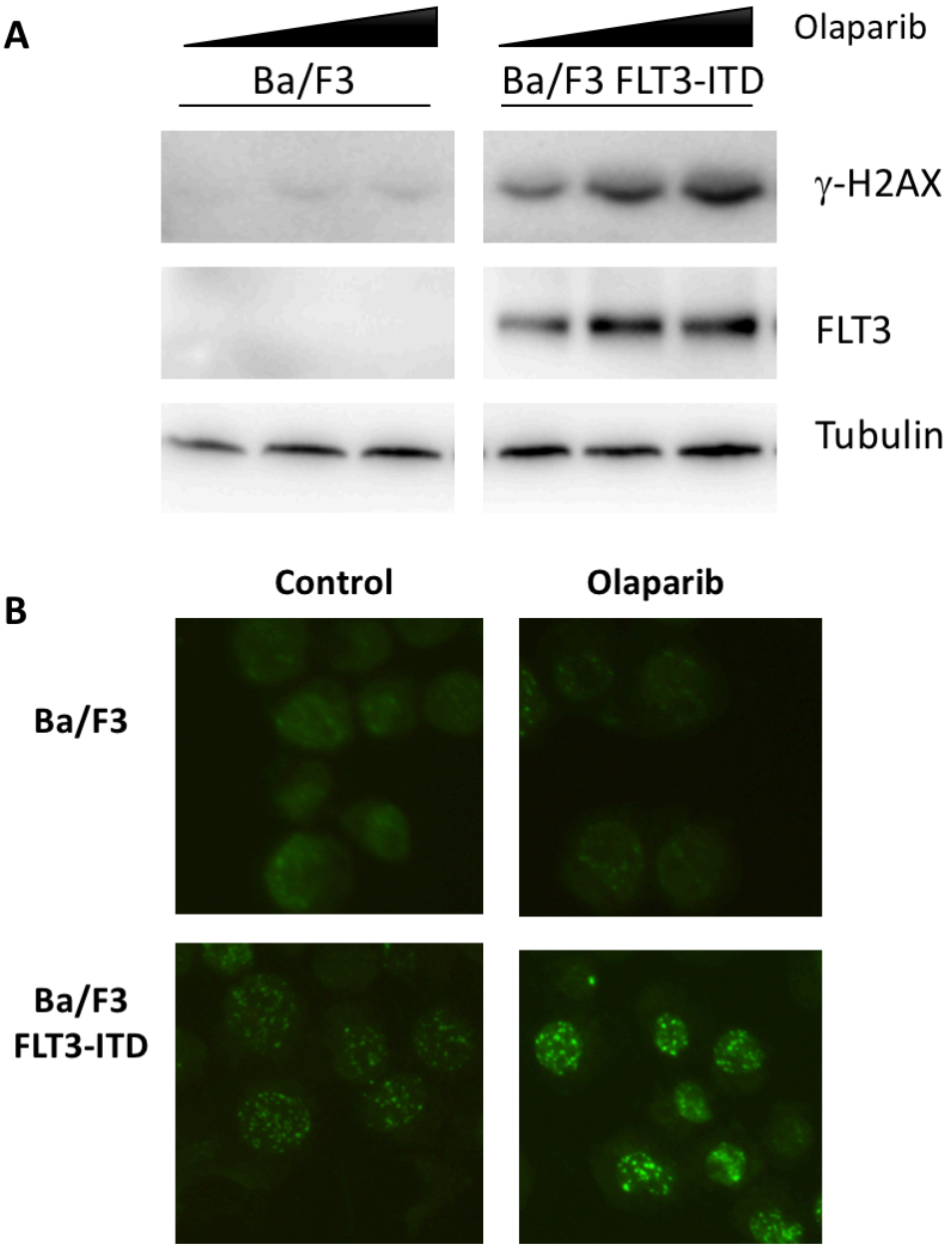
A
Olaparib
Ba/F3
Ba/F3 FLT3-ITD
γ-H2AX
FLT3
Tubulin
B
Control
Olaparib
Ba/F3
Ba/F3
FLT3-ITD

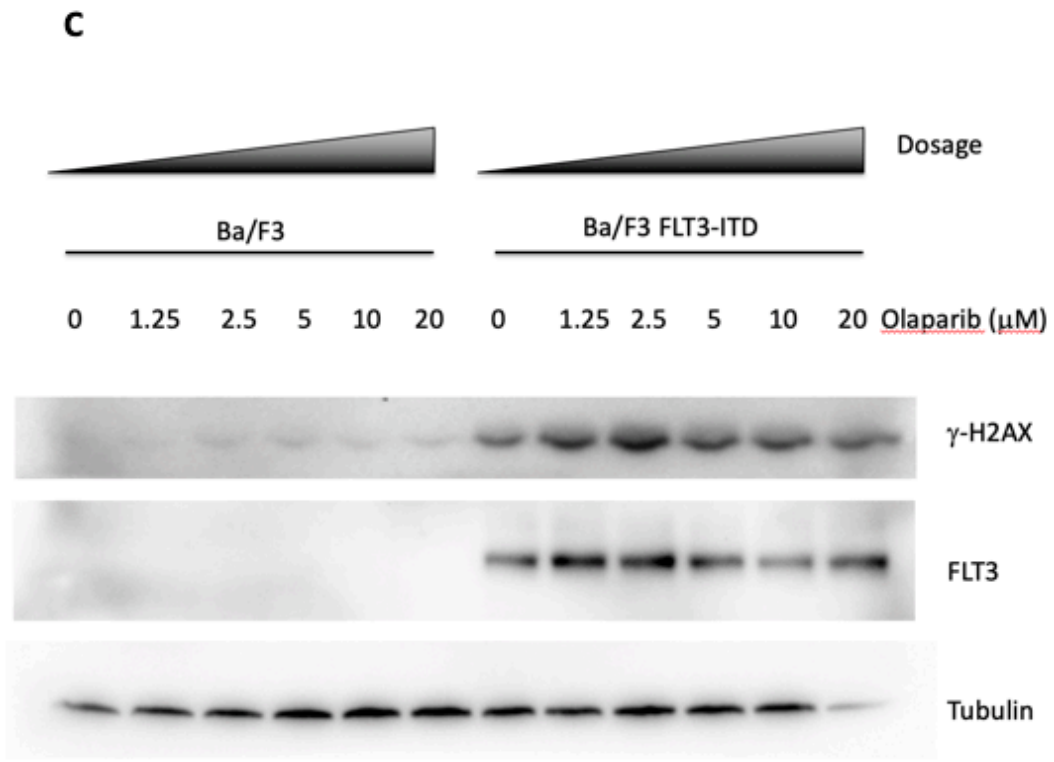

Figure 5.2 Analysis of γ–H2AX level in Ba/F3 FLT3-ITD cells treated with Olaparib by immunoblot analysis and immunofluorescence microscopy.

Ba/F3 FLT3-ITD cells and the Ba/F3 control line were treated with of Olaparib. The cells were harvested after 24 hours for immunoblot and immunofluorescence analysis. **(A)** Representative immunoblot result with increasing dose of Olaparib at 1 and 2.5 μM of Olaparib. The **(B)** Representative immunofluorescence image captured with Olympus IX70 using 40X objective. n=3. **(C)** Original immunoblot of **(A).**

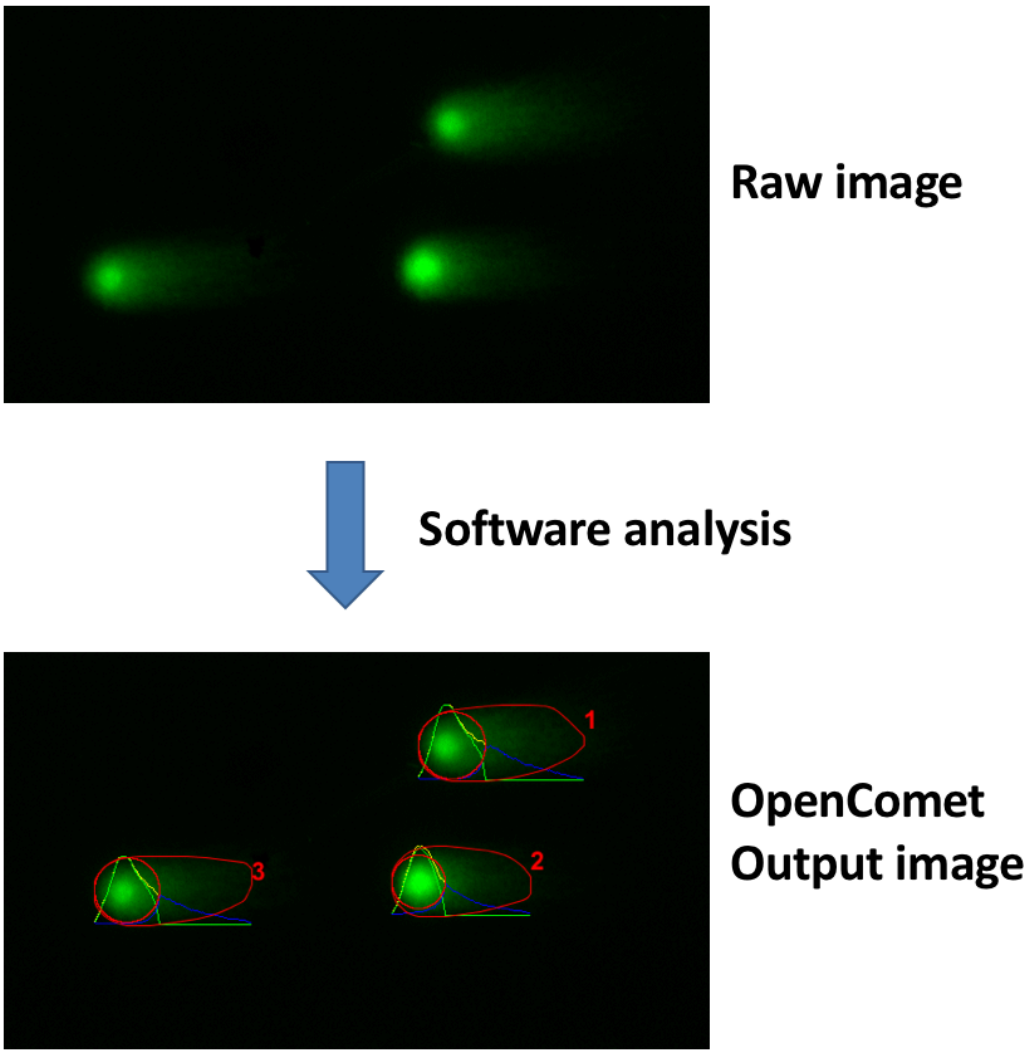

Figure 5.3 Diagrammatic illustration of neutral comet assay analysis using OpenComet Software.

The raw comet image was imported to OpenComet plugin in ImageJ and the analysis was run automatically. Individual comet was identified by the Comet Head Finding Algorithm as shown in the figure as 1, 2 and 3. The olive circle represented whole comet and the regular circle represented comet head. The tail moment was calculated as the length of comet tail times tail DNA %.

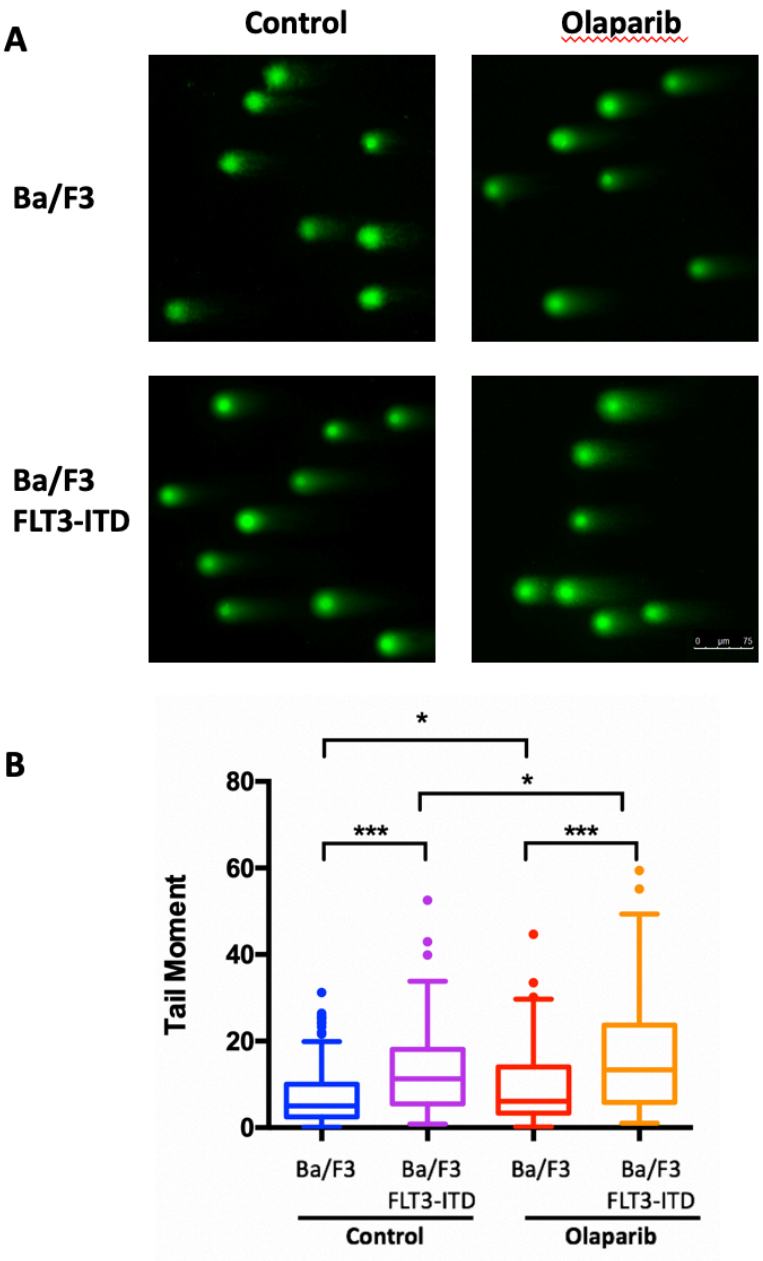

Figure 5.4 Neutral comet assay in Ba/F3 FLT3-ITD cells treated with Olaparib. The cells were treated with 1 µM of Olaparib for 24 hours and subjected to neutral comet assay to detect DNA double-stranded breaks. **(A)** Representative comet images. White bar = 75 mm. **(B)** Statistical analysis of comet images using the OpenComet software. The double-stranded DNA breaks were quantified by tail moment (% of DNA tail x length of tail). * $p < 0.05$; *** $p < 0.001$. N=3 and n=117; 113; 102 & 112 respectively.

5.4 Elevated ROS level modulated sensitivity of FLT3-ITD to PARP inhibitor

To identify the cause of increased DSB in FLT3-ITD AML, intracellular ROS was measured in Ba/F3 FLT3-ITD. The level of ROS was significantly higher in FLT3-ITD compared with its parental control (Fig. 5.5). Intriguingly, Olaparib treatment accentuated the increase in ROS in Ba/F3 FLT3-ITD cells but not the parental control.

5.5 Combination of PARP inhibitors and chemotherapy

The result of defective HR repair and anti-leukemic effect of PARPi in FLT3-ITD AML suggested that it might be used to sensitize leukemic cells to chemotherapy. The effects of Olaparib in combination with chemotherapy were evaluated in MOLM-13 NSG xenograft model (see Chapter 3.13). Leukemia engraftment was monitored at real-time by bioluminescence imaging after intraperitoneal luciferin injection. Olaparib in combination with chemotherapy suppressed leukemic growth *in vivo* (Fig. 5.6). However, the small number of animals in each group had precluded robust statistical evaluation.

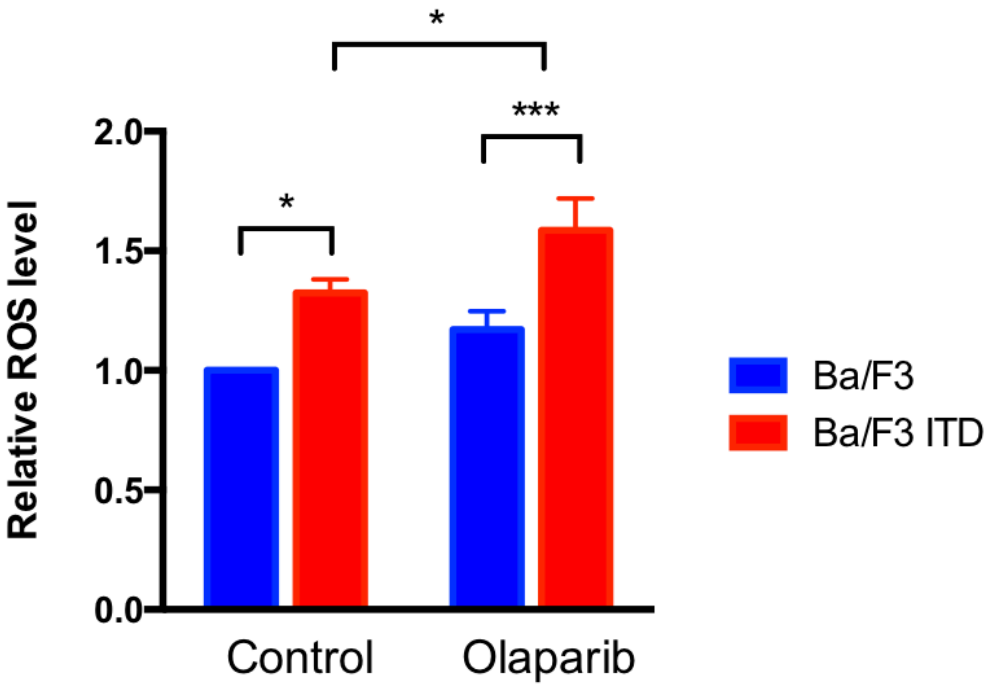

Figure 5.5 Intracellular ROS measurement of Ba/F3 FLT3-ITD cells treated with Olaparib.

Ba/F3 parental and FLT3-ITD cells were treated with Olaparib for 24 hours and followed by loading of ROS detecting probe 2'7'-dichlorodihydro-fluorecein diacetate (H2DCFDA). The intracellular ROS level was measured by flow cytometry and normalized to Ba/F3 parental vehicle control. n=3, * $p < 0.05$; *** $p < 0.001$.

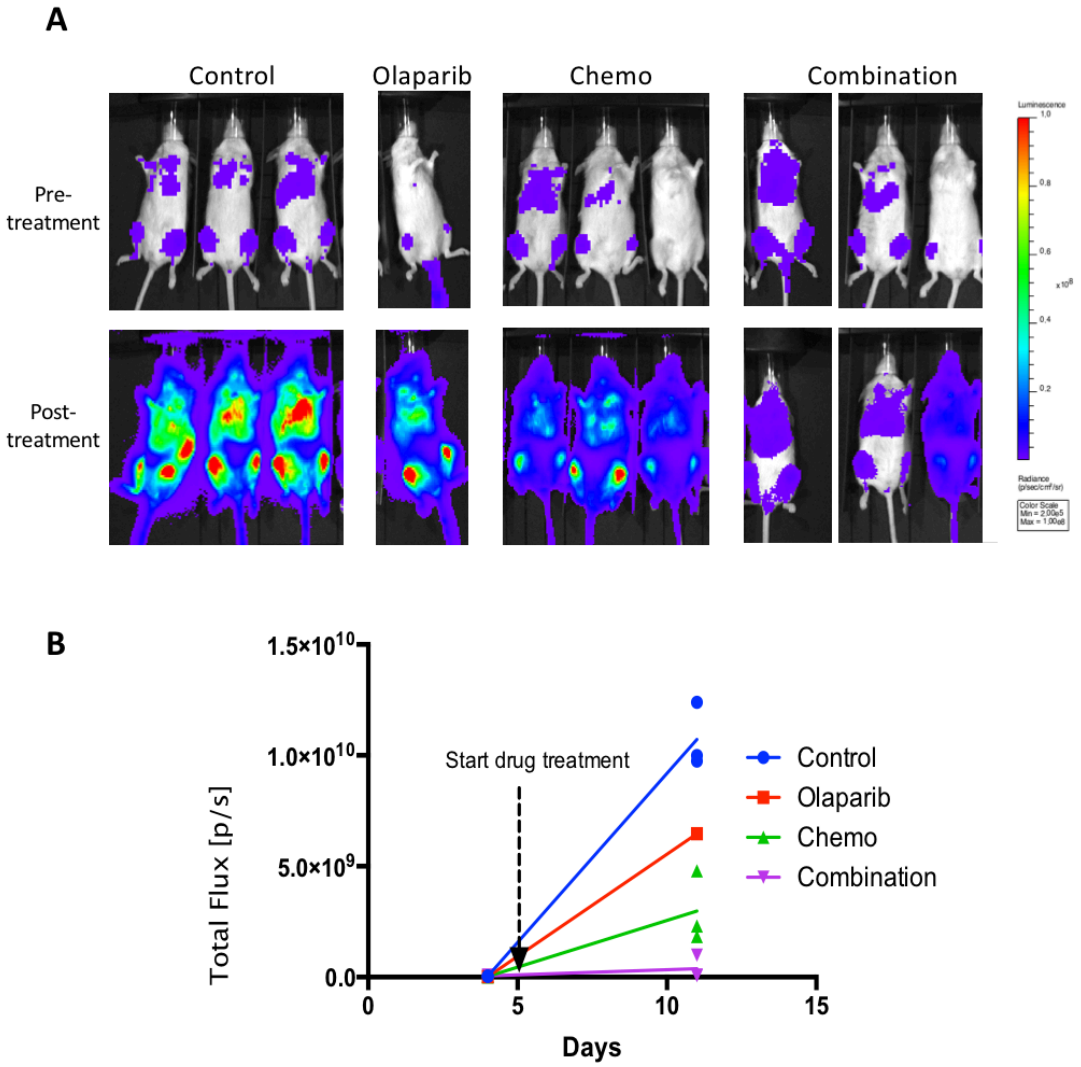

Figure 5.6 *In vivo* drug treatment of Olaparib and chemotherapy in MOLM-13 xenograft model.

(A) MOLM-13 AML cells transduced with a luciferase reporter were intravenous injected into NSG mice. The pre-treatment bioluminescence image was captured at 4-day post-transplantation. At the 5th day of the experiment, mice were divided into 4 groups for drug treatment for 5 days. The post-treatment image was taken at 11th day post-transplantation. The experiment was terminated due to cytotoxic effect of chemo drugs. **(B)** The graph showing the change in luminescence intensity with individual experimental mouse.

Chapter 6 Screening of synthetic lethal candidate of DDR genes with PARP inhibitors by *shRNA* library screen

The works described in the previous chapters has led to identification of PARP inhibitor Olaparib as a potential therapeutic agent in FLT3-ITD AML. However, the effects of Olaparib were generally modest and more effective regimen comprising Olaparib and its therapeutic partners were needed. This could be accomplished by a comprehensive *shRNA*-based screening and was based on the principle of synthetic lethality.

6.1 Methodology

The DDR *shRNA* library consisted of all reported genes with functions annotated to DDR pathways from publications and published databases KEGG and REPAIRtoire [8,14,15,17,18,89,90]. A total of 248 genes were included in this study. The screening was performed in collaboration with Dr. Johannes Zuber (Research Institute of Molecular Pathology, Vienna) [88]. List of clinical trials involving DDR inhibitors was summarized in Appendix 4 [78]. The workflow of the procedure was shown in Figure 6.1.

6.2 Characterization and generation of *Flt3^{ITD} Npm1^{c+}* cell line

To generate murine *Flt3 $^{ITD/+}$ Npm1 $^{c/+}$* leukemic cell line, spleen cells from *Flt3 $^{ITD/+}$ Npm1$^{c/+}$* double knockin mouse (generously provided by Dr. George S Vassiliou, Sanger Institute, UK) were transplanted into recipient mice to develop AML [105]. Once AML occurred, BM cells were isolated and established into a stable and proliferating cell line. The immunophenotypes of leukemic cells in BM, spleen and liver of the

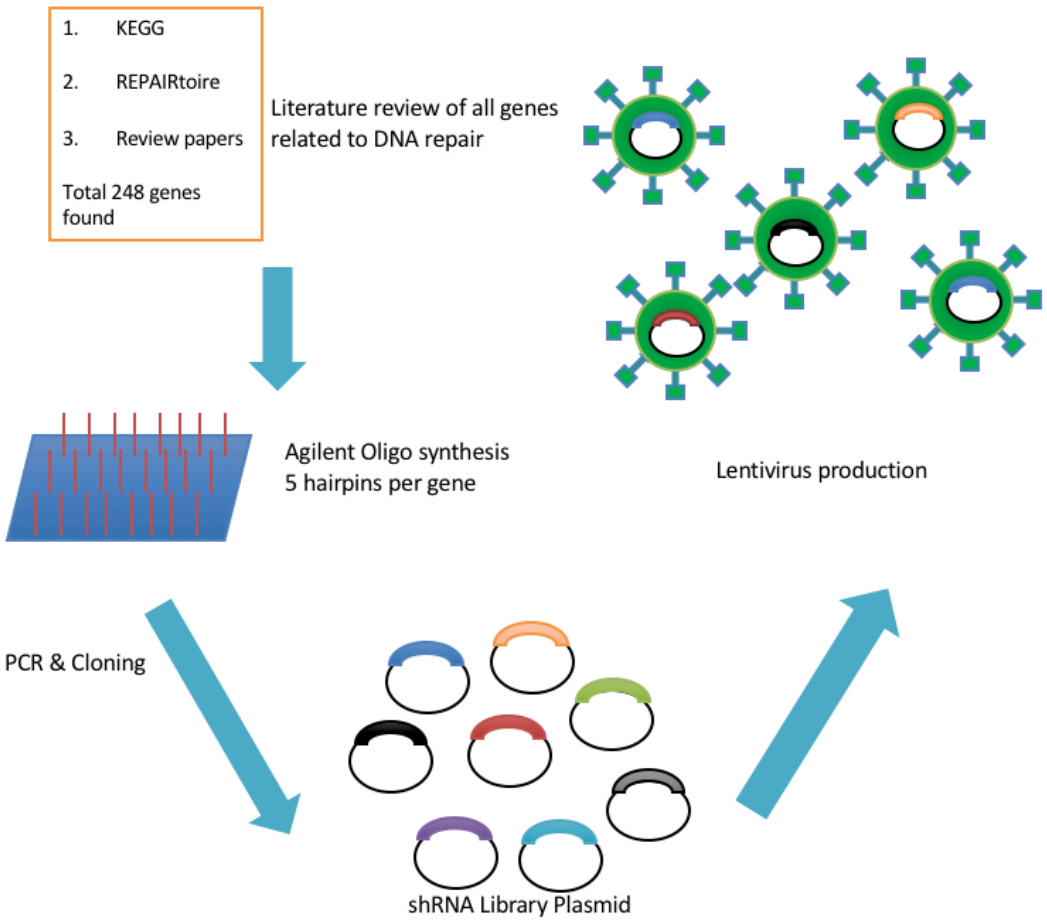

Figure 6.1 Construction of mouse DDR *shRNA* library.

Based on literature review, a total of 248 genes with reported DNA damage response were selected. Top 5 hairpins of each gene were selected for oligo synthesis. Following the cloning of *shRNA* library plasmid, the DDR *shRNA* library was packaged into lentivirus for subsequent experiments.

recipient mice were shown in Figure 6.2, showing a predominant mature granulocytic (Gr-1^+/ $Mac1^+$), monocytic (Gr-1^-/$Mac1^+$) and immature myelomoncytic (c-kit^+) populations, resembling the immunophenotype in previous publication [105]. Those of the AML cell line established *in vitro* were shown in Figure 6.3. and they were all Mac-1^+ / Gr-1^+ mature granulocytic leukemic cells, indicating successful establishment of a *Flt3* $^{ITD/}$ *Npm1* $^{c/+}$ myeloid-lineage leukemic cell line. The *in vitro* effects of Olaparib on their clonogenicity were examined. Olaparib suppressed the colony forming ability of the *Flt3* $^{ITD/+}$*Npm1* $^{c/+}$ leukemic cells more significantly than the MLL-AF9 transformed AML cells (Fig. 6.4).

6.3 Experimental scheme of DDR *shRNA* screening *in vivo*

The experimental scheme was designed with the purpose of screening for novel therapeutic agents that could work synergistically with Olaparib (Fig. 6.5). *Flt3* $^{ITD/+}$ *Npm1* $^{c/+}$ AML cells were transduced with lentivirus carrying *pRRL-GFP-Puro-mouse DDR-shRNA*. AML cells that were successfully transduced were purified by FACS 2 days post-transduction and transplanted into recipient mice intravenously. Two weeks post-transplantation, one group of recipient mice were treated with Olaparib (50mg/kg) intraperitoneally for 2 weeks and another group received vehicle control (same volume of DMSO solvent control) by the same route and for the same duration. All mice were euthanized and analyzed 4 weeks after completion of the 2-week treatment or if they showed symptoms of debilitation which was most likely related to underlying AML. Genomic DNA was extracted from their BM samples and Miseq sequencing library was prepared as per protocol from Dr. Johnannes Zuber. The list of DNA samples submitted for sequencing was shown in Appendix 5. Diagrammatic representation of the final PCR product of Miseq sequencing library was shown in

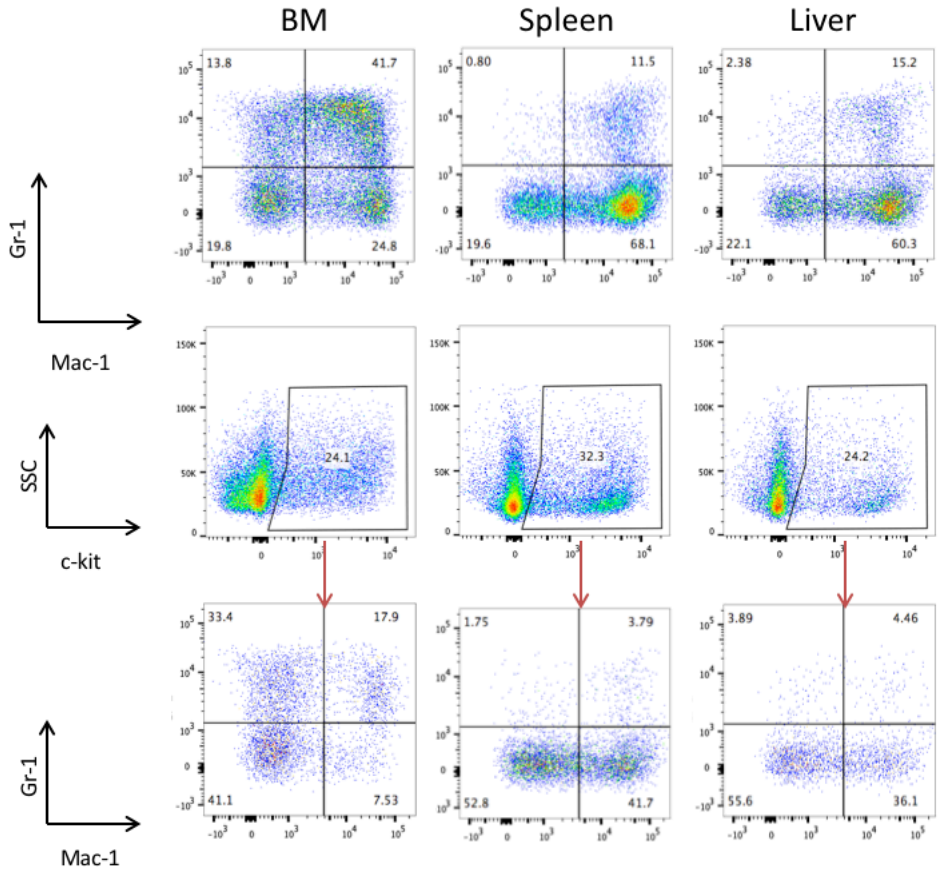

Figure 6.2 Immunophenotype analysis of leukemic mice transplanted with spleen cells recovered from *Flt3*$^{ITD/+}$ *Npm1*$^{c+/+}$ knockin mouse.

Representative flow cytometry data of *Flt3* $^{ITD/+}$ *Npm1* $^{c/+}$ leukemic cells gated on CD45.2 population of bone marrow (BM), spleen and liver cells of the recipient mice. Result showed that the leukemic cells resided in BM were predominantly Mac-1^{+} / Gr-1^{+} mature granulocytic cells while leukemic cells resided in spleen and liver were Gr-1^{-} / Mac1^{+}monocytic cells.

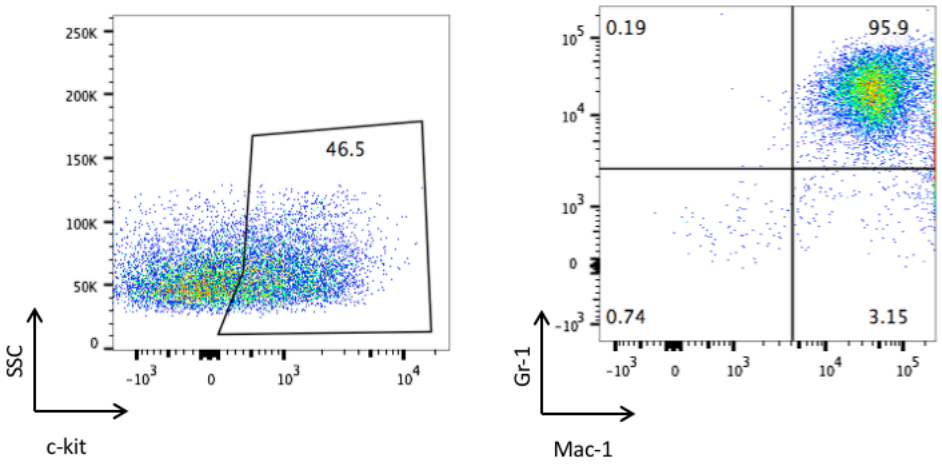

Figure 6.3 Immunophenotype analysis of primary murine *Flt3* $^{ITD/+}$ *Npm1* $^{c/+}$ cell line.

Representative flow cytometry data of the *in vitro* established *Flt3* $^{ITD/}$ *Npm1* $^{c/+}$ leukemic cells line. Result showed that the cell line was predominantly Mac-1^{+} / Gr-1^{+} mature granulocytic cells and around half of those cells were c-kit^{+}.

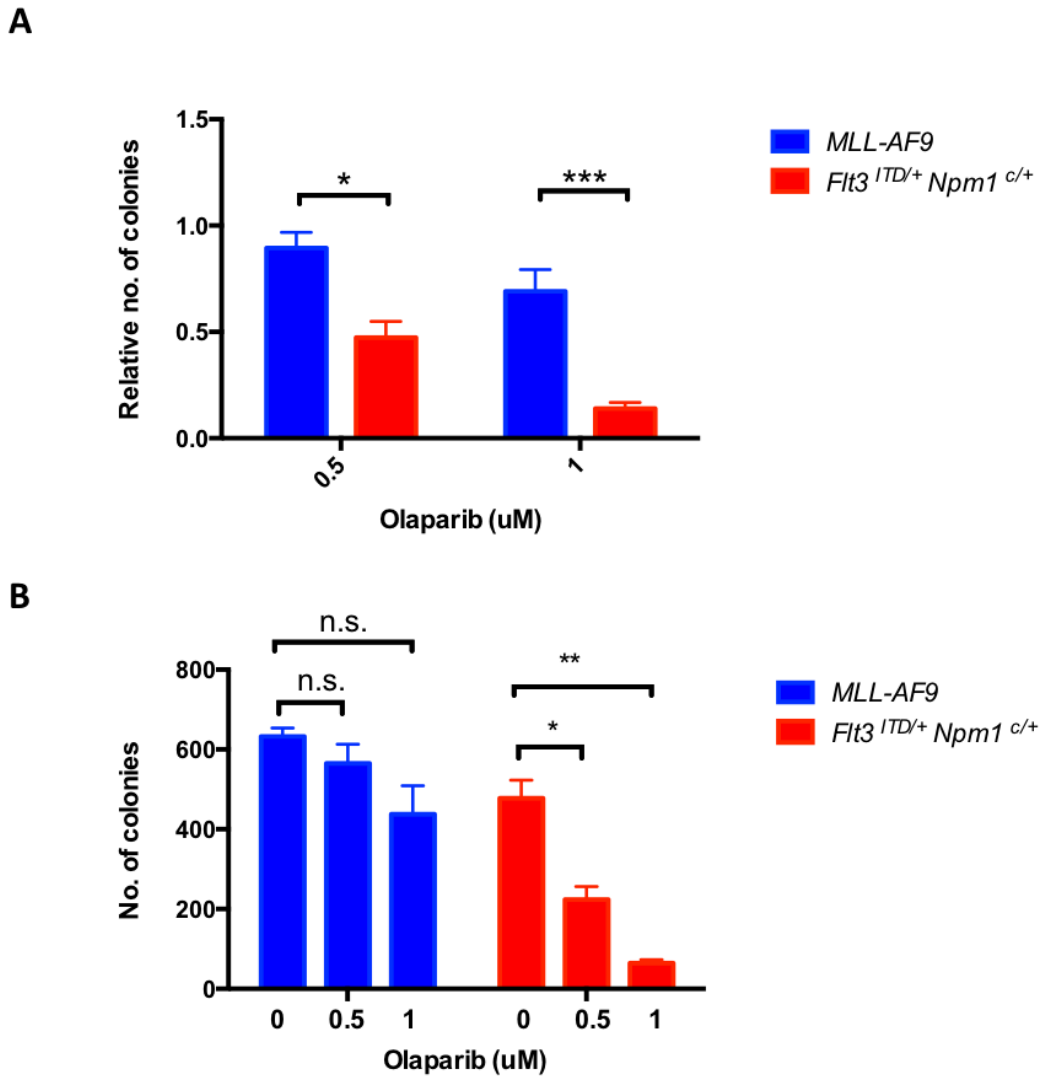

Figure 6.4 Colony formation assay of leukemic cells of *MLL-AF9* or *Flt3$^{ITD/+}$ Npm1$^{c/+}$* treated with Olaparib for 5 days in methyl cellulose.

(A) Relative no. of colonies normalized to vehicle control and **(B)** Absolute no. of colonies. n=3, * $p < 0.05$; ** $p < 0.01$; *** $p < 0.001$; n.s. not significant.

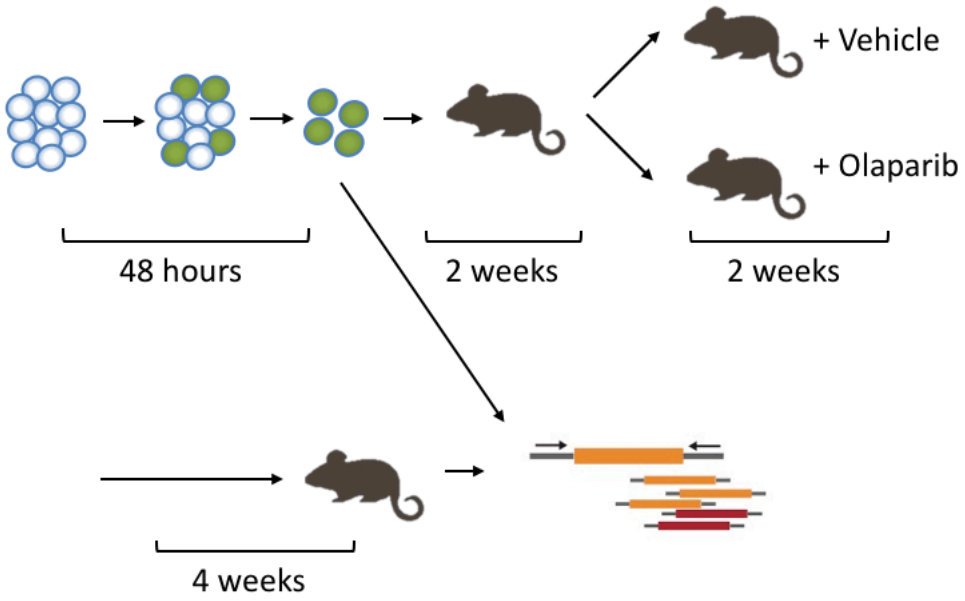

Figure 6.5 Experimental scheme of *in vivo shRNA* library screening.

The *Flt3* $^{ITD/+}$ *Npm1* $^{c/+}$ leukemic cells were lentivirally transduced with mouse DDR library *shRNA*s. At 48th hours post-transduction, the GFP+ transduced cells were sorted out by FACS and 0.1 million of sorted cells were transplanted into each recipient CD45.1 SJL mouse. Two weeks post-transplantation, the experimental mice were divided into two groups and treated with either 50mg/kg Olaparib or vehicle control for 2 weeks. The drug-resistant clones were allowed to recover for 4 additional weeks *in vivo*. The genomic DNA of total bone marrow leukemic cells were harvested, together with the pre-transplant samples to prepare sequencing library for Miseq run.

Figure 6.6A. Prior to Miseq sequencing, the pooled final PCR product was subjected to Sanger sequencing using Illumina P5 adaptor primer to confirm correct amplification of *shRNA* hairpin region, unique barcoding region and custom sequencing primer binding site (Figure 6.6B). The sequencing library was sequenced by Illumina Miseq platform using Miseq V2 50 cycle kit.

6.4 Basic bioinformatics filtering of the MiSeq run

Basic bioinformatics analysis, including FASTQC of sequencing run, trimming of reads, de-multiplexing and mapping of *shRNA* hairpins and statistical analysis were performed by Ms Claire Lynn. The FASTQC confirmed the 22bp reads of *shRNA* hairpins followed by the common sequencing adapter and unique barcodes (Fig. 6.7). With the spiking of 20% PhiX control DNA, the remaining 80% of the reads were uniquely mapped to the *shRNA* library, indicating that the Miseq run was successful.

The mapping of unique *shRNA* hairpins showed that the starting material, the *pRRL-GFP-puro-mouse DDR shRNA library* plasmid (#14), contained all 1240 unique mouse DDR *shRNA* hairpins (Fig. 6.8A). Similarly, most unique hairpins were detected in the pre-transplantation samples (#1 & 7) and were mapped to 1235 and 1228 unique hairpins respectively. The number of unique hairpins was decreased in endpoint samples, indicating that cells carrying those hairpins were dropped out overtime.

The quality filtered mapped reads of individual samples were shown in Figure 6.8B. The number of reads that would give a good representation of hairpins distribution

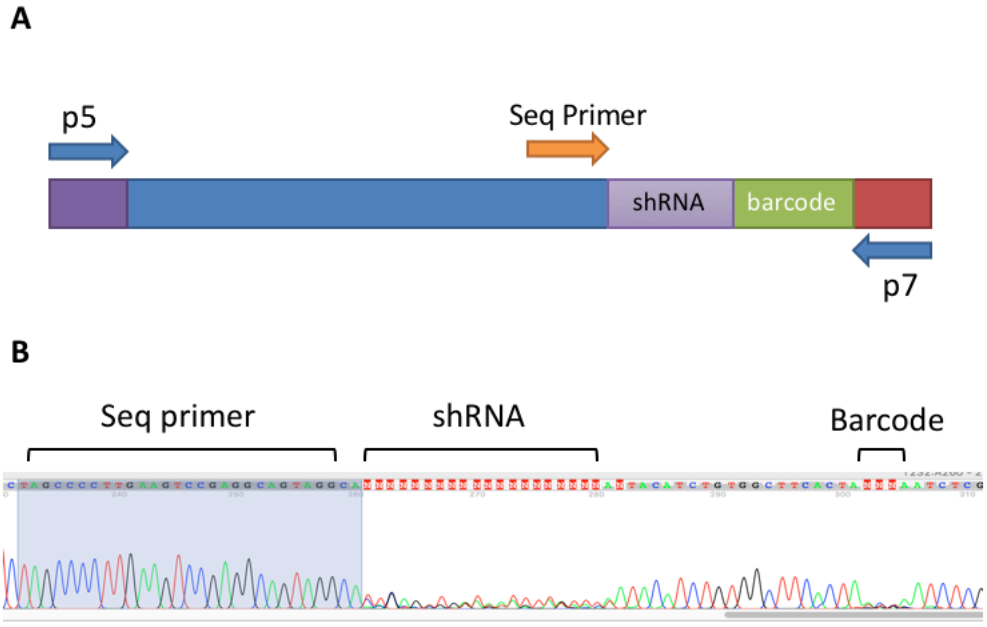

Figure 6.6 Information of DNA sample for Miseq.

(A) Diagram showing the final PCR product generated for Miseq sequencing. **(B)** Chromatogram of the final pooled DNA sample by Sanger sequencing using Illumina P5 sequencing primer.

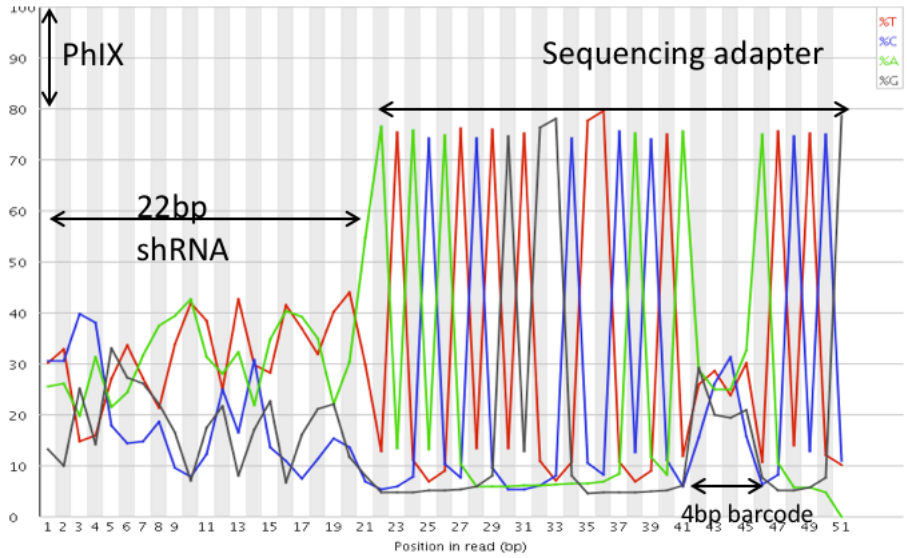

Figure 6.7 FASTQC plot of the Miseq sequencing run.

The diagram showed the read alignment of pooled sequencing reads with the 20% PhiX control DNA filtered out. Starting from read position 1-22 was the unique *shRNA* sequences following by the common sequencing adapter from position 23-50. The unique 4bp barcodes marked individual samples.

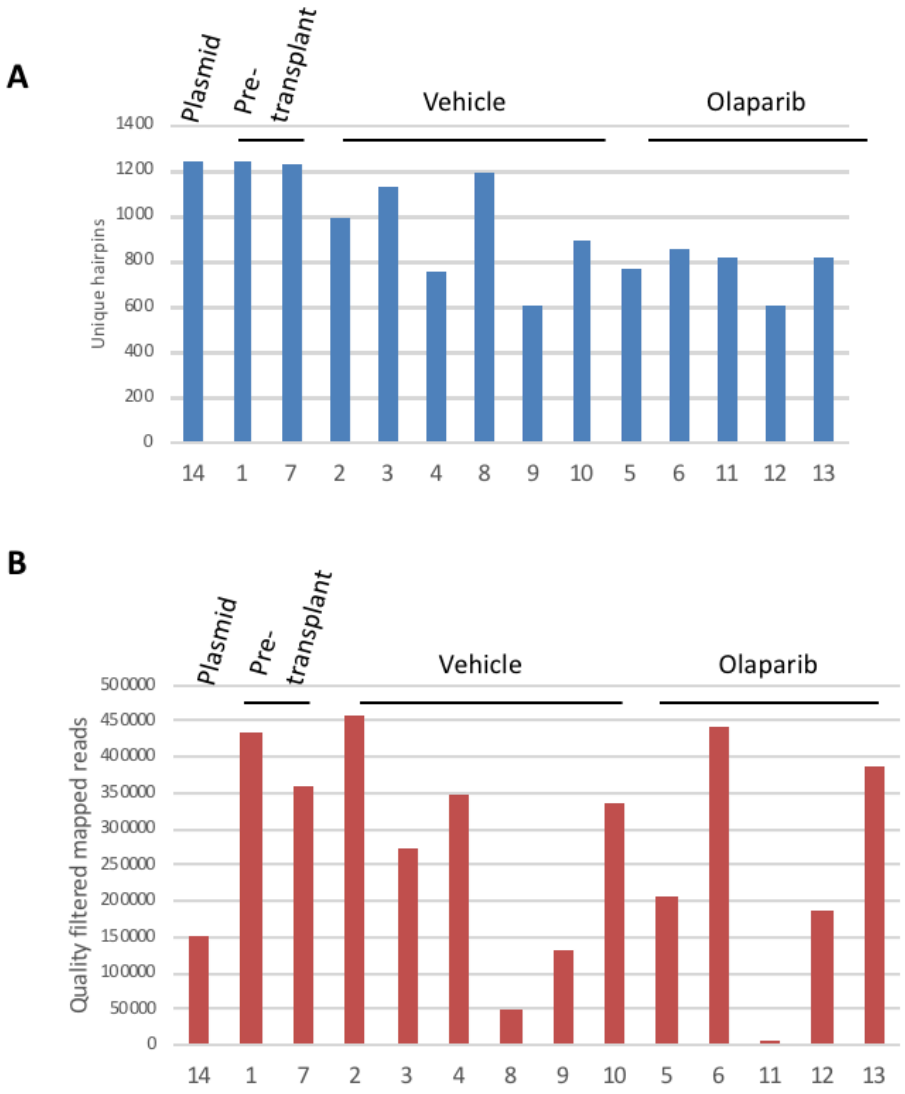

Figure 6.8 Alignment result of Miseq run to unique hairpin sequences.

(A) Result of mapping of reads to unique hairpins. Total number of hairpins in the mouse DDR library was 1240. **(B)** Result of mapping the quality filtered mapped reads.

was 1000-fold of the number of total hairpins, i.e. 1.2 x 10^6 reads. In this study, the number of reads of individual samples ranged from 7397 (#11) to 0.46 x 10^6 (#2) (Fig. 6.8B). Cutoff for downstream analysis was set to 0.12 x 10^6 reads. Therefore, sample # 8 and 11, with 47,197 and 7,397 mapped reads, were not included for further analysis.

6.5 Dropout analysis of *shRNA* library screening

Analysis of *shRNA* screen was performed using an open-source processing pipeline optimized for analyzing pooled library sequencing screens in edgeR[106]. The overall distribution of probability of hairpin dropout was shown in Figure 6.9.

A gene was considered as dropped out if the probability of hairpin dropout (Pdrop) ≥ 0.6, i.e. 3 out of 5 hairpins of that gene were significantly dropped out (p-value < 0.05) compared with pre-transplant samples. There were 206 dropout genes in Olaparib-treated group and 70 in the vehicle-treated group. To identify genes that were dropped out preferentially in Olaparib-treated group, the group specific dropout was examined based on the probability of dropout Olaparib minus vehicle-treated (Pdrop of O-V) of which the cutoff threshold was set at ≥ 0.6 (Figure 6.10), i.e. at least 3 out of 5 hairpins of the same gene were dropped out in the Olaparib-treated group compared with the vehicle-treated group.

183 genes were dropped out in both vehicle-treated and Olaparib-treated leukemic cells (Fig. 6.10). They were considered candidates with oncogenic potential independent of the effects of Olaparib, including genes that were important for cell survival in general as well as those for leukemogenesis of $Flt3^{ITD/+}Npm1^{c/+}$ AML cells.

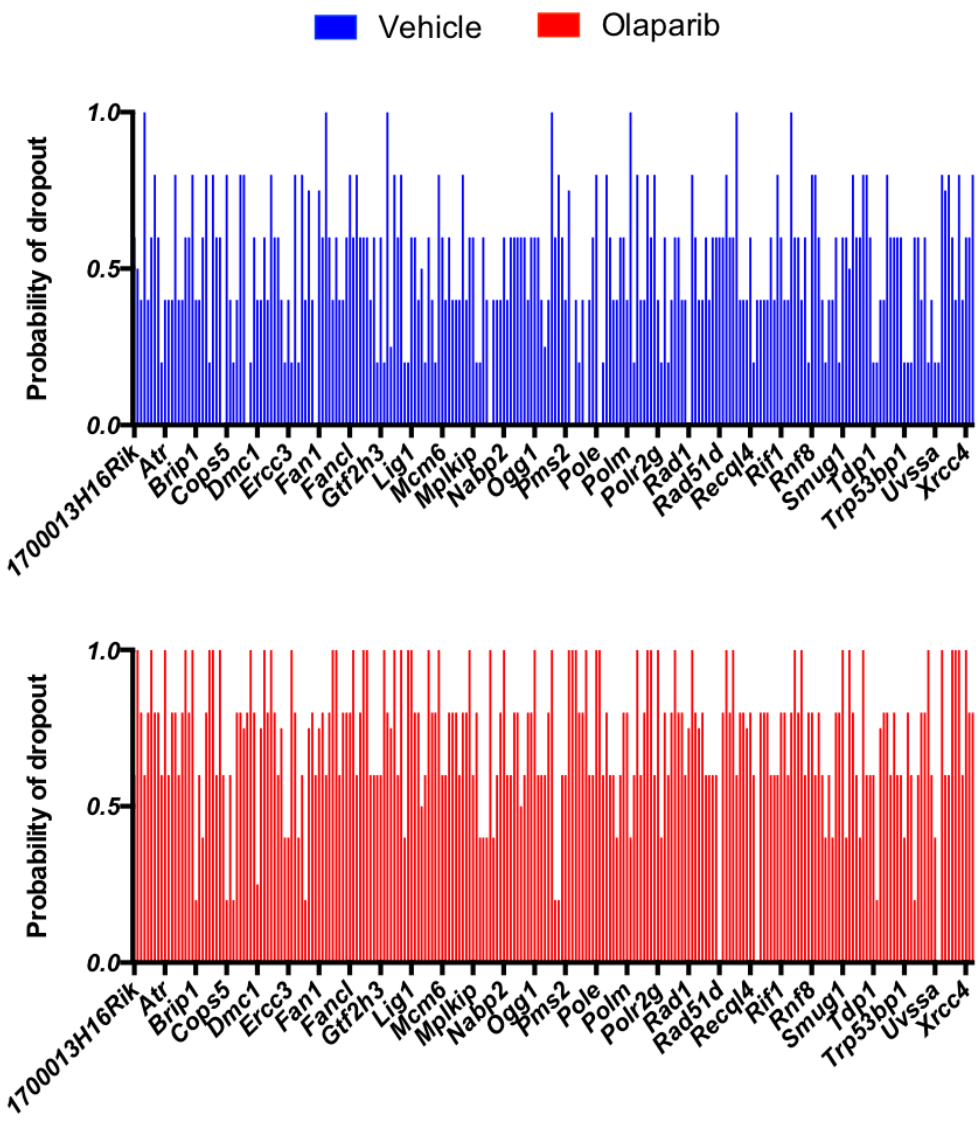

Figure 6.9 Overall distribution of probability of gene dropout in the *shRNA* screen.

Distribution plots showing the probability of dropout of all murine DDR genes in the *shRNA* screening. Top plot was overall distribution of dropout of comparing *in vivo* vehicle-treated endpoint samples verse pre-transplant samples while bottom plot showed the result of *in vivo* Olaparib-treated endpoint samples versus pre-transplant samples.

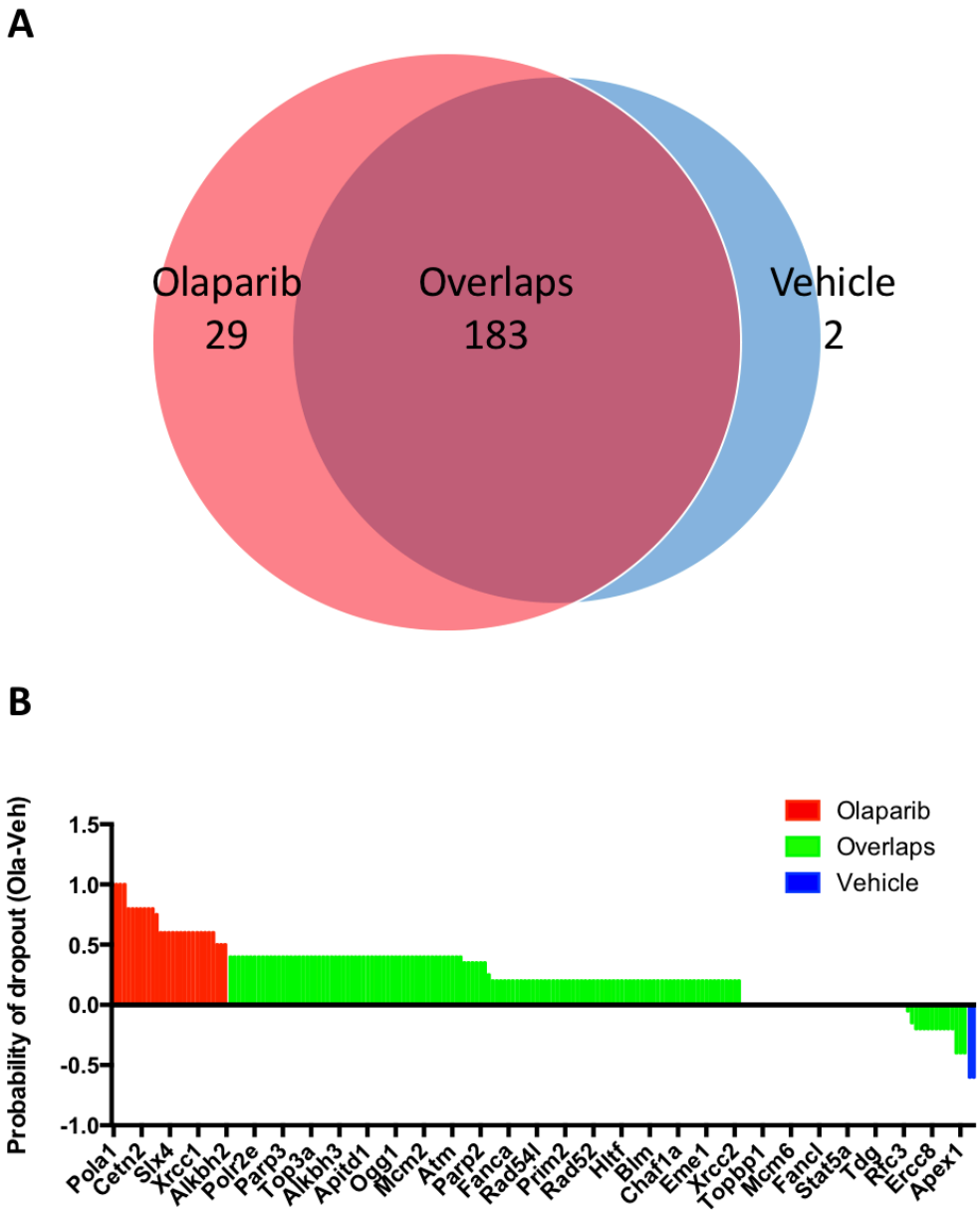

Figure 6.10 Distribution of unique hairpin dropouts.

(A) Venn diagram showing the number of unique gene dropouts in vehicle-treated group (2), Olaparib-treated group (29) and the overlaps gene dropouts (183). **(B)** The plot showing the difference of probability dropout of Olaparib-treated group and vehicle-treated group.

The dropout probability of important DDR genes was listed in Appendix 6. Surprisingly, HR genes such as *Brca2* were categorized in the common dropout group because the baseline cutoff of Pdrop was set at 0.6 (Appendix 7). Nevertheless, all 5

hairpins of *Brca2* were dropped out in Olaparib-treated group while 3 hairpins were dropped out in the control group, demonstrating the effectiveness of targeting *Brca2*-down-regulated clones using Olaparib.

29 genes were dropped out specifically in the Olaparib-treated group (Fig. 6.10). They were enriched in checkpoint factors and DNA replication factors (Fig. 6.11). For instance, members of the Family B Polymerase are involved in nuclear DNA replications and they include Polymerase alpha (α), delta (δ) and epsilon (ε) (Appendix 5) [107-109]. The *Atr* (ATM and rad3-related) gene encodes a master regulator kinase that is activated by replication stress and single stranded DNA damage [110-112].

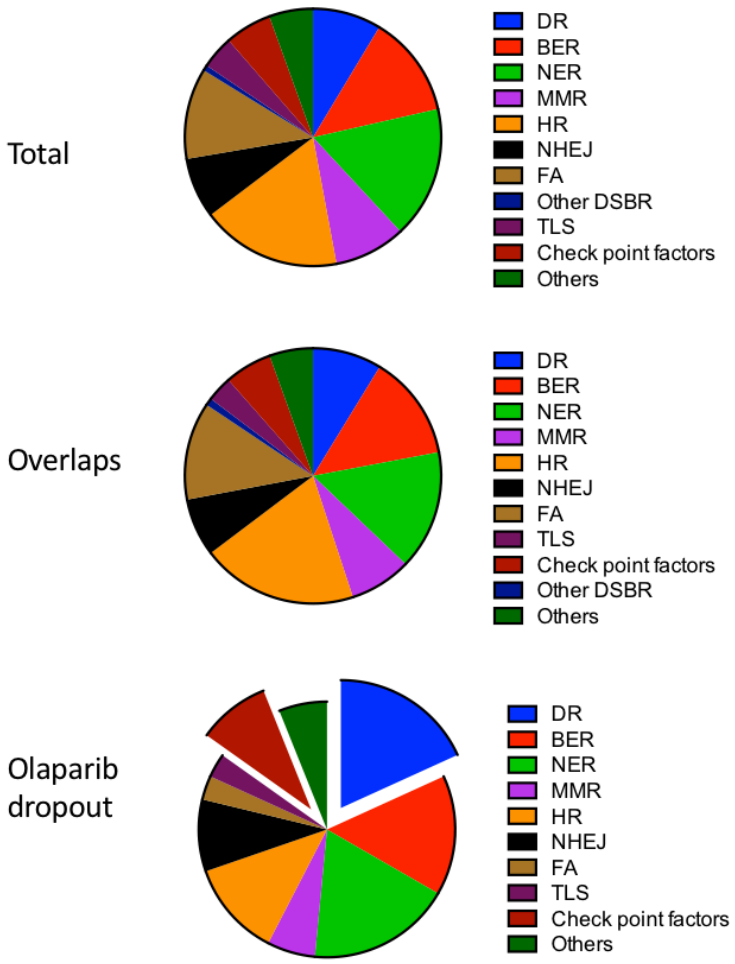

Figure 6.11 Pie chart of overall distribution of dropout genes categorized by their role in DNA damage response pathways.

Top chart showed the percentage of total DDR library genes sorted by DNA repair pathways, and similar distribution was found in the Middle chart: the overlap group. The percentage of check point factors and DNA repair genes were increased in Olaparib droupout drop (Bottom chart).

Abbreviations: DR (DNA repair); BER (base excision repair); NER (nucleotide excision repair); MMR (mismatch repair); HR (homologous recombination); NHEJ (non-homologous end-joining); FA (fanconi anemia); Other DSBR (double stranded breaks repair); TLS (translesion repair)

Chapter 7. Summary and Discussions

Despite their diversity of clinicopathologic, cytogenetic abnormalities and genetic mutations, current treatment for AML has been uniform [1,3-6]. *FLT3-ITD* is one of the most common mutations in cytogenetically normal AML with higher relapse rates and poorer overall survivals. Although clinical studies have shown the effectiveness of multi-kinase or specific FLT3 inhibitors in clearing myeloblasts from blood and BM, the response was invariably transient [61-65]. There is an urgent need to develop novel effective strategy for this AML subtype.

The research began by the observation that *BRCA2* expression was significantly suppressed in primary AML samples and human AML cell lines carrying *FLT3-ITD* as well as mouse B-lymphoid Ba/F3 cells transduced with *FLT3-ITD*, consistent with the GSE15434 gene expression data deposited by Dugas's group in University of Münster. *BRCA2* was regulated by FLT3-ITD signaling and its expression could be restored by a specific FLT3 inhibitor quizartinib. On the other hand, defective HR repair was evident by Traffic Light Reporter assay. Increased DSB was demonstrated by increased γ-H2AX staining as well as the neutral comet assay and was likely secondary to an increase in ROS. The results have shed important lights to the pathogenesis of FLT3-ITD AML and were of clinical significance to the development of therapeutic strategies for this AML subtype.

This study highlighted the importance of defective DDR in the pathogenesis of FLT3-ITD AML. The results were consistent with published data about defective DDR in this subtype, but the underlying mechanisms were reportedly different among studies. In this study, it was associated with down-regulation of *BRCA2* expression and HR. On the other hand, down-regulation of *Ku70* and *Ku80*, key components of classical

NHEJ pathway and up-regulation of *DNA ligase IIIα*, key enzyme in alt-NHEJ pathway component, have been reported in both FLT3-ITD AML cell lines and mouse *Flt3-ITD* knockin model [74]. Paradoxically, increase in *RAD51* expression and HR activity have also been reported in FLT3-ITD AML [20,103,113]. Very recently, both HR and NHEJ, but not the alt-NHEJ pathway, were shown to be dependent on FLT3 signaling [20]. Differences in cell line models and the use of FLT3 inhibitors in terms of doses and timing might have contributed to the different observations. These discrepancies notwithstanding, our study provided functional readout of HR and NHEJ, showing defective HR but not NHEJ in an isogenic Ba/F3 FLT3-ITD cell model.

Results arising from this study were of clinical relevance. PARP inhibitors have been shown effective in the treatment of *BRCA* mutant breast and ovarian cancers [75,76], a condition known as synthetic lethality in which PARP becomes a therapeutic target when DSB repair is defective due to *BRCA* mutation. Similarly, the observations that *BRCA2* expression was down-regulated in FLT3-ITD AML supported the proposition that PARP inhibitors might be an effective treatment. In fact, Olaparib suppressed leukemia cell proliferation and clonogenicity in both Ba/F3 FLT3-ITD and *Flt3* $^{ITD/+}$ *Npm1*$^{c/+}$ cell line models. Combination of Olaparib and chemotherapy was also effective in reducing leukemia growth *in vivo* based on small number of animals studied so far. Intriguingly, treatment of Olaparib further increased the intracellular ROS level. There were also emerging evidences that DNA damage could induce ROS generation through the H2AX-Nox1-Rac1 pathway [114], uncovering a mechanistic link of two dysregulated pathways in FLT3-ITD AML. Therefore, it is possible that the PARP inhibitor Olaparib not only increased the level of DSB but also induced more

ROS stress, generating a feedback loop to induce more DSB. These observations supported a selectively toxic effect of Olaparib towards FLT3-ITD AML cells.

The experimental model developed in this study might provide important foundation for larger scale genomic studies. Specifically, an *in vivo* DDR *shRNA* library dropout screening based on a mouse *Flt3*$^{ITD/}$ *Npm1*$^{c/+}$ double knockin model was designed to identify potential therapeutic targets that might become effective when used in combination with Olaparib. First, the nuclear DNA replication Family B Polymerase was particularly enriched as dropout candidates. While DNA polymerases are not a good target in cancer therapy, antimetabolite such as cytarabine that interferes with DNA replication, is widely used as the frontline induction therapy for AML patients. This finding further consolidated the proposal of adding Olaparib to standard "7+3" chemotherapy for FLT3-ITD AML patients. Second, clinical trials of ATR inhibitors are currently in Phase 1/2 for advanced solid tumors as a single agent and in combination with chemotherapy, radiotherapy and PARP inhibitors [115]. Functional studies are ongoing to validate these results and the database will provide leads for future mechanistic and clinical studies.

There are a number of limitations in this study. The importance of proving decrease in BRCA2 at the protein level was not neglected and multiple optimizations and antibodies had been used to detect BRCA2 protein, yet it remained problematic to detect this high molecular weight protein in primary AML samples. It is of urgent need to obtain this critical data in primary samples. BRCA2 protein level would also be compared among human AML cell lines and isogenic 32D and Ba/F3 lines transduced with *FLT3-ITD*. Furthermore, FLT3 inhibitor quizartinib restored *BRCA2* expression, supporting the proposition that *BRCA2* transcription was regulated by FLT3-ITD

signaling. Therefore, further experiments using the *Tet-on-pLKO* doxycycline inducible *shRNA* system (Addgene #21915) would be performed to demonstrate the direct link between *FLT3* and *BRCA2.* How FLT3-ITD signaling suppressed *BRCA2* remained unknown and future work by means of transcriptomic and proteomic analysis as well as *BRCA2* promoter region by chromatin immunoprecipitation (ChIP)-PCR and ChIP-seq should be considered.

Another technical challenge in the study of FLT3-ITD AML was the need of robust models in both *in vitro* and *in vivo* studies. The commonly used model included mouse pro-B Ba/F3 cells and 32D myeloblast cells that overexpressed *FLT3-ITD* oncogene and proliferated independent of ambient IL3, with the caveat that they were not strictly leukemic [12,70,71,73,74,93,103,104,116,117]. Patients-derived FLT3-ITD AML cell lines MOLM-13 and MV-4-11 have also been compared with other human AML cell lines carrying wildtype FLT3. However, these cell lines might have accumulated various mutations during repeated passages and might not truly represent the biology of the original AML from which they were derived. *Flt3-ITD* knockin mouse model has been generated by inserting an *ITD* mutation into the juxtamembrane domain of murine *Flt3* allele, resulting in a myeloproliferative state [92,118]. Concurrent oncogenic events could cooperate with Flt3-ITD to develop *bona fide* AML model in mice. These oncogenic events included conditional knockout of *Runx1*, *Dmnt3a* and knockin of *Npm1* type A mutation [105,116,119-122]. Thus, the murine $Flt3^{ITD/+}$ $Npm1^{c/+}$ leukemic cell line was generated for the *shRNA* screening. Further experiments that include control cell lines without FLT3-ITD signaling should be performed to identify FLT3-ITD specific targets.

In summary, the work described in this thesis demonstrated increased DSB in FLT3-ITD AML due to increase in ROS production and defective DDR efficiency and fidelity due to reduced *BRCA2* down-regulation and HR activity (Fig. 7.1). The latter was exploited as a potential therapeutic target as evident by the use of PARP inhibitor Olaparib, singly or in combination with conventional chemotherapy in this AML subtype. This information would become a solid foundation for future mechanistic and translational studies in FLT3-ITD AML.

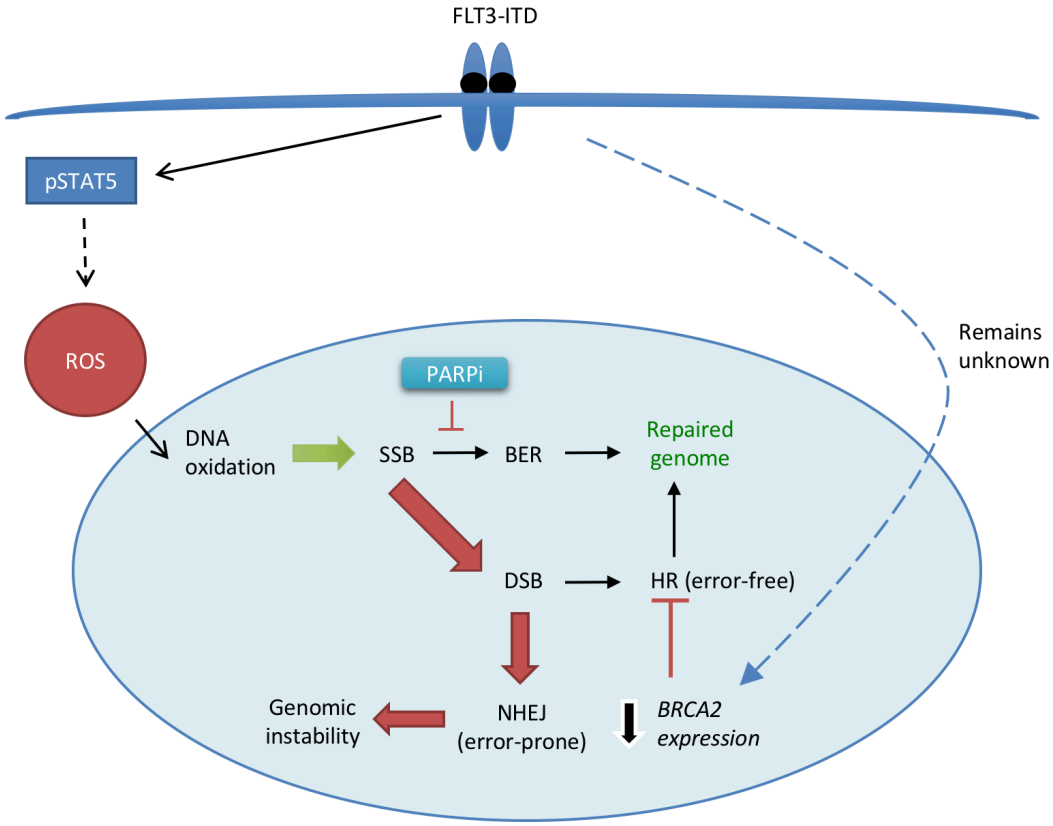

Figure 7.1. Diagrammatic summary of work.

ITD mutation in FLT3 receptor caused constitutive activation of FLT3 signaling and led to ligand-independent phosphorylation of STAT5. The FLT3-ITD-STAT5 pathway increased ROS generation which oxidized genomic DNA and hence SSB formation. On the other side, FLT3-ITD down-regulated *BRCA2* expression and impaired the DSB repair via the error-free HR pathway. The inhibition of BER by PARPi resulted in accumulation of SSB during DNA replication and thus led to formation of DSB. The unrepaired DSB was mainly repaired by error-prone NHEJ and led to genomic instability.

Appendix

Appendix 1 Culture conditions of human AML cell lines.

Cell lines	*FLT3* status	Key mutation	Cell passage density	Culture medium
MOLM-13	*WT/ITD*	*MLL-AF9*	0.3 x 10^6/ mL	RPMI+10% FBS
MV-4-11	*ITD/ITD*	*MLL-AF4*	0.3 x 10^6/ mL	IMDM+10% FBS
NOMO-1	*WT/WT*	*MLL-AF9*	0.5 x 10^6/ mL	RPMI+10% FBS

Appendix 2 List of primers used for RT-QPCR.

qPCR primer	Forward	Reverse
ATM	CCAAATCCCTCCACCTGCAT	AGAACACACATTGGATAGTGGT
ATR	ACTGCTTGTTATGACAGGGCT	GTCCACTCGGACCTGTTAGC
BRCA1	GTCCCATCTGTCTGGAGTTGA	AAAGGACACTGTGAAGGCCC
BRCA2	AGCACTCCAGATGGCACAATA	TTCTTGACCAGGTGCGGTAAA
CHEK1	AGGGGTGGTTTATCTGCATGG	CTGTTGCCAAGCCAAAGTCT
CHEK2	AAGCCTTAAGACACCCGTGG	CGACTAGTAGAAGGCTGGGC
DNA-PK	GAGAAGGCGGCTTACCTGAG	AGCGCCCTTATACATTAGCAT
P53	TGACACGCTTCCCTGGATTG	TTTTCAGGAAGTAGTTTCCATAGGT
PARP1	AGCTCCCAGGAGTCAAGAGT	GTCGTTCTGAGCCTTTAGGG
GAPDH	AGGGCTGCTTTTAACTCTGGT	CCCCACTTGATTTTGGAGGGA
mBrca2	AGATAGGCCTGAGACTTCCTT	TGTGGTTCATAACCGTGGGG
mGapdh	TGGCCTTCCGTGTTCCTAC	GAGTTGCTGTTGAAGTCGCA

Appendix 3 List of antibodies used.

Antibody	Dilution	Company
Rabbit anti-total FLT3	1:500	Santa Cruz Biotechnology, USA
mouse anti-γ-H2AX (ser139)	1:2000	Millipore
Mouse anti-β–actin	1:5000	Sigma, USA

Appendix 4 Clinical trials involving DDR inhibitors

Target	Agent	Phase	Cancer(s) enrolled	Trial identifier
DNA-PK	MSC2490484A	I	Solid tumors, CLL	NCT02316197
	MSC2490484A	I	Solid tumors	NCT02516813
	VX-984	I	Solid tumors	NCT02644278
ATM	AZD0156	I	Solid tumors	NCT02588105
ATR	VX-970 ± chemotherapy	I	Solid tumors	EudraCT: 2013-005100-34
		I	Solid tumors	NCT02157792
		II	Ovarian, primary peritoneal or Fallopian tube	NCT02595892
		I	Solid tumors	NCT02595931
		II	Advanced gynecologic cancers	NCT02627443
		I/II	Advanced NSCLC, SCLC, Gynae or neuroendocrine	NCT02487095
		II	Advanced urothelial	NCT02567409
	VX-970 ± RT	I	Locally advanced HNSCC	NCT02567422
		I	NSCLC brain metastases	NCT02589522
	VX-970 + targeted therapy	I	Solid tumors	NCT02723864
	AZD6738	I	Relapsed CLL, PLL, B-cell lymphomas	NCT01955668
	AZD6738 ± chemotherapy	I	Solid tumors, HNSCC, ATMloss NSCLC, gastric or GOJ carcinoma	NCT02264678
		I	Solid tumors	NCT02630199
	AZD6738 + RT	I	Solid tumors	NCT02223923
CHK1	MK8776 (SCH 900776)	II	Relapsed AML	NCT01870596
		I	Relapsed lymphoma	NCT00779584
		I	Relapsed AML	NCT00907517
CHK1/2	LY2603618	I/II	NSCLC	NCT01139775
		I/II	Pancreatic carcinoma	NCT00839332
		II	NSCLC	NCT00988858
		I	Solid tumors	NCT01296568
		I	Solid tumors	NCT01341457
		I	Solid tumors	NCT00415636
	CCT245737	I	Solid tumors	NCT02797964
		I	Solid tumors	NCT02797977
	GDC-0575 ± chemotherapy	I	Solid tumors, relapsed lymphoma	NCT01564251
	LY2606368	II	Refractory SCLC	NCT02735980
		II	Ovarian, breast, prostate	NCT02203513
		II	Solid tumors	NCT02873975
		I	Solid tumors	NCT01115790
		I	Solid tumors	NCT02778126
		I	Solid tumors	NCT02514603
		I	Pediatric solid tumors	NCT02808650
	LY2606368 + chemotherapy	I	Relapsed AML, high risk MDS	NCT02649764
		I	Solid tumors	NCT02124148
	LY2606368 + targeted therapy	I	Solid tumors	NCT02860780
	LY2606368 + RT	I	Locally advanced HNSCC	NCT02555644

WEE1	AZD1775	II	SCLC	NCT02593019
		I	Solid tumors	NCT01748825
		I	Solid tumors	NCT02482311
		I	Solid tumors	NCT02610075
	AZD1775 + chemotherapy	II	Ovarian, TP53mut	NCT01357161
		II	Ovarian, TP53mut, or platinum resistant	NCT01164995
		II	Ovarian, primary peritoneal, or fallopian	NCT02101775
		II	NSCLC, 1st line	NCT02087241
		II	NSCLC, 2nd line	NCT02087176
		II	NSCLC	NCT02513563
		II	Gastric carcinoma	NCT02448329
		II	HNSCC	NCT02196168
		I/II	Pancreatic	NCT02194829
		I/II	Pediatric solid tumors	NCT02095132
		I	Locally advanced HNSCC	NCT02508246
		I	Solid tumors	NCT00648648
	AZD1775 + targeted therapy	I	Solid tumors	NCT02511795
			AML, other myeloid malignancies	NCT02381548
	AZD1775 + RT	I/II	Pancreatic	NCT02037230
		I	HNSCC	NCT02585973
		I	Locally advanced cervical cancer	NCT01958658
		I	GBM	NCT01849146
		I	Pediatric DIPG	NCT01922076
	AZD1775 + immune checkpoint inhibitor	I	Solid tumors	NCT02617277
BER	TRC102	I	Solid tumors, lymphoma	NCT01851369
	TRC102 + chemotherapy	II	GBM	NCT02395692
		I/II	Solid tumors	NCT02535312
		I	Solid tumors	NCT00692159
		I	Hematologic malignancies	NCT01658319
	TRC102 + RT	I	NSCLC	NCT02535325

Adapted from [78].

Appendix 5 Miseq sequencing run samples.

Seq ID	Experiment	Type	Description
1	1	*in vivo*	GFP sorted, pre-transplant sample
2	1	*in vivo*	End point; BM #1; vehicle
3	1	*in vivo*	End point; BM #2; vehicle
4	1	*in vivo*	End point; BM #3; vehicle
5	1	*in vivo*	End point; BM #5; Olaparib 50mg/kg
6	1	*in vivo*	End point; BM #6; Olaparib 50mg/kg
7	2	*in vivo*	GFP sorted, pre-transplant sample
8	2	*in vivo*	End point; BM #1; vehicle
9	2	*in vivo*	End point; BM #2; vehicle
10	2	*in vivo*	End point; BM #3; vehicle
11	2	*in vivo*	End point; BM #4; Olaparib 50mg/kg
12	2	*in vivo*	End point; BM #5; Olaparib 50mg/kg
13	2	*in vivo*	End point; BM #6; Olaparib 50mg/kg
14	/	plasmid	*pRRL GFP puro*; Mouse DDR library plasmid

Appendix 6 Candidate dropout gene list specific to Olaparib treatment.

Gene	Probability of dropout			Role in DNA damage response signalling									
	Veh.	Ola.	Diff.	DR	BER	NER	MMR	HR	NHEJ	FA	TLS	Check point factors	Others
Msh5	0	1	1				✓						
Pola1	0	1	1	✓									
Pold2	0	1	1				✓						
Pole2	0	1	1	✓	✓	✓							
Cetn2	0.2	1	0.8			✓							
Dclre1c	0	0.8	0.8						✓				
Ddb1	0.2	1	0.8			✓							
Ercc4	0.2	1	0.8			✓							
Gtf2h4	0.2	1	0.8			✓							
Hus1	0.2	1	0.8									✓	
Ung	0.2	1	0.8		✓								
Rad1	0	0.75	0.75									✓	
Mcm4	0.2	0.8	0.6	✓									
Mre11a	0.2	0.8	0.6					✓	✓				
Polb	0.2	0.8	0.6		✓				✓				
Rnf4	0.2	0.8	0.6					✓					
Slx4	0.2	0.8	0.6					✓					
Ube2a	0.2	0.8	0.6								✓		
Atr	0.4	1	0.6									✓	
Clk2	0	0.6	0.6		✓								
Fam175a	0	0.6	0.6					✓					
Fancd2	0.4	1	0.6							✓			
Pola2	0.4	1	0.6	✓									
Polr2g	0.4	1	0.6			✓							
Rnaseh2c	0.4	1	0.6	✓									
Xrcc1	0.4	1	0.6		✓								
Alkbh2	0.5	1	0.5	✓									
H2afx	0.25	0.75	0.5										✓
Sprtn	0.5	1	0.5										✓

Abberviations: Veh. (vehicle); Ola. (Olaparib); Diff. (difference); DR (DNA repair); BER (base excision repair); NER (nucleotide excision repair); MMR (mismatch repair); HR (homologous recombination); NHEJ (non-homologous end-joining); FA (fanconi anemia); Other DSBR (double stranded breaks repair); TLS (translesion repair)

Appendix 7 Dropout probability of important DDR genes in the screening.

Gene	Probability of dropout			Dropout group	Role in DNA damage response signalling							
	Veh.	Ola.	Diff.		DR	BER	NER	MMR	HR	NHEJ	FA	Check point factors
Atm	0.2	0.6	0.4	Common								✓
Atr	0.4	1	0.6	Ola.								✓
Brca1	0.4	0.8	0.4	Common					✓		✓	
Brca2	0.6	1	0.4	Common					✓		✓	
Chek1	0.6	0.6	0	Common								✓
Chek2	0.6	1	0.4	Common								✓
Lig3	0.6	0.8	0.2	Common		✓						
Lig4	0.4	0.8	0.4	Common						✓		
Mre11a	0.2	0.8	0.6	Ola.					✓	✓		
Nbn	0.4	0.6	0.2	Common					✓			
Prkdc	0.4	0.8	0.4	Common						✓		
Rad50	0.6	0.6	0	Common					✓	✓		
Rad51	0.4	0.6	0.2	Common					✓		✓	
Rpa1	0.8	0.6	-0.2	Common			✓	✓	✓			
Trp53	0.6	0.6	0	Common								✓

Abberviations: Veh. (vehicle); Ola. (Olaparib); Diff. (difference); DR (DNA repair); BER (base excision repair); NER (nucleotide excision repair); MMR (mismatch repair); HR (homologous recombination); NHEJ (non-homologous end-joining); FA (fanconi anemia); Other DSBR (double stranded breaks repair); TLS (translesion repair)

Reference

1 Cancer Genome Atlas Research, N. *et al.* Genomic and epigenomic landscapes of adult de novo acute myeloid leukemia. *N Engl J Med* **368**, 2059-2074, doi:10.1056/NEJMoa1301689 (2013).

2 Vardiman, J. W. *et al.* The 2008 revision of the World Health Organization (WHO) classification of myeloid neoplasms and acute leukemia: rationale and important changes. *Blood* **114**, 937-951, doi:10.1182/blood-2009-03-209262 (2009).

3 Vogler, W. R. *et al.* A phase III trial comparing idarubicin and daunorubicin in combination with cytarabine in acute myelogenous leukemia: a Southeastern Cancer Study Group Study. *J Clin Oncol* **10**, 1103-1111, doi:10.1200/JCO.1992.10.7.1103 (1992).

4 Berman, E. *et al.* Results of a randomized trial comparing idarubicin and cytosine arabinoside with daunorubicin and cytosine arabinoside in adult patients with newly diagnosed acute myelogenous leukemia. *Blood* **77**, 1666-1674 (1991).

5 Wiernik, P. H. *et al.* A multicenter trial of cytarabine plus idarubicin or daunorubicin as induction therapy for adult nonlymphocytic leukemia. *Semin Oncol* **16**, 25-29 (1989).

6 Vogler, W. R., Velez-Garcia, E., Omura, G. & Raney, M. A phase-three trial comparing daunorubicin or idarubicin combined with cytosine arabinoside in acute myelogenous leukemia. *Semin Oncol* **16**, 21-24 (1989).

7 Cornelissen, J. J. & Blaise, D. Hematopoietic stem cell transplantation for patients with AML in first complete remission. *Blood* **127**, 62-70, doi:10.1182/blood-2015-07-604546 (2016).

8 Ciccia, A. & Elledge, S. J. The DNA damage response: making it safe to play with knives. *Mol Cell* **40**, 179-204, doi:10.1016/j.molcel.2010.09.019 (2010).

9 David, S. S., O'Shea, V. L. & Kundu, S. Base-excision repair of oxidative DNA damage. *Nature* **447**, 941-950, doi:10.1038/nature05978 (2007).

10 Khanna, K. K. & Jackson, S. P. DNA double-strand breaks: signaling, repair and the cancer connection. *Nat Genet* **27**, 247-254, doi:10.1038/85798 (2001).

11 Schar, P. Spontaneous DNA damage, genome instability, and cancer--when DNA replication escapes control. *Cell* **104**, 329-332 (2001).

12 Sallmyr, A., Fan, J. & Rassool, F. V. Genomic instability in myeloid malignancies: increased reactive oxygen species (ROS), DNA double strand breaks (DSBs) and error-prone repair. *Cancer Lett* **270**, 1-9, doi:10.1016/j.canlet.2008.03.036 (2008).

13 Kushner, B. H. *et al.* High risk of leukemia after short-term dose-intensive chemotherapy in young patients with solid tumors. *J Clin Oncol* **16**, 3016-3020, doi:10.1200/JCO.1998.16.9.3016 (1998).

14 Jackson, S. P. & Bartek, J. The DNA-damage response in human biology and disease. *Nature* **461**, 1071-1078, doi:10.1038/nature08467 (2009).

15 Mills, K. D., Ferguson, D. O. & Alt, F. W. The role of DNA breaks in genomic instability and tumorigenesis. *Immunol Rev* **194**, 77-95 (2003).

16 Coutts, A. S. & La Thangue, N. The p53 response during DNA damage: impact of transcriptional cofactors. *Biochem Soc Symp*, 181-189 (2006).

17 Mandal, P. K., Blanpain, C. & Rossi, D. J. DNA damage response in adult stem cells: pathways and consequences. *Nat Rev Mol Cell Biol* **12**, 198-202, doi:10.1038/nrm3060 (2011).
18 Esposito, M. T. & So, C. W. DNA damage accumulation and repair defects in acute myeloid leukemia: implications for pathogenesis, disease progression, and chemotherapy resistance. *Chromosoma* **123**, 545-561, doi:10.1007/s00412-014-0482-9 (2014).
19 Helleday, T., Petermann, E., Lundin, C., Hodgson, B. & Sharma, R. A. DNA repair pathways as targets for cancer therapy. *Nat Rev Cancer* **8**, 193-204, doi:10.1038/nrc2342 (2008).
20 Maifrede, S. *et al.* Tyrosine kinase inhibitor-induced defects in DNA repair sensitize FLT3(ITD)-positive leukemia cells to PARP1 inhibitors. *Blood*, doi:10.1182/blood-2018-02-834895 (2018).
21 Karanam, K., Kafri, R., Loewer, A. & Lahav, G. Quantitative live cell imaging reveals a gradual shift between DNA repair mechanisms and a maximal use of HR in mid S phase. *Mol Cell* **47**, 320-329, doi:10.1016/j.molcel.2012.05.052 (2012).
22 Sinha, S., Villarreal, D., Shim, E. Y. & Lee, S. E. Risky business: Microhomology-mediated end joining. *Mutat Res* **788**, 17-24, doi:10.1016/j.mrfmmm.2015.12.005 (2016).
23 Truong, L. N. *et al.* Microhomology-mediated End Joining and Homologous Recombination share the initial end resection step to repair DNA double-strand breaks in mammalian cells. *Proc Natl Acad Sci U S A* **110**, 7720-7725, doi:10.1073/pnas.1213431110 (2013).
24 Lamarche, B. J., Orazio, N. I. & Weitzman, M. D. The MRN complex in double-strand break repair and telomere maintenance. *FEBS Lett* **584**, 3682-3695, doi:10.1016/j.febslet.2010.07.029 (2010).
25 Dickey, J. S. *et al.* H2AX: functional roles and potential applications. *Chromosoma* **118**, 683-692, doi:10.1007/s00412-009-0234-4 (2009).
26 Rogakou, E. P., Pilch, D. R., Orr, A. H., Ivanova, V. S. & Bonner, W. M. DNA double-stranded breaks induce histone H2AX phosphorylation on serine 139. *J Biol Chem* **273**, 5858-5868 (1998).
27 Gaymes, T. J., Mufti, G. J. & Rassool, F. V. Myeloid leukemias have increased activity of the nonhomologous end-joining pathway and concomitant DNA misrepair that is dependent on the Ku70/86 heterodimer. *Cancer Res* **62**, 2791-2797 (2002).
28 Brady, N., Gaymes, T. J., Cheung, M., Mufti, G. J. & Rassool, F. V. Increased error-prone NHEJ activity in myeloid leukemias is associated with DNA damage at sites that recruit key nonhomologous end-joining proteins. *Cancer Res* **63**, 1798-1805 (2003).
29 Slupianek, A. *et al.* Fusion tyrosine kinases induce drug resistance by stimulation of homology-dependent recombination repair, prolongation of G(2)/M phase, and protection from apoptosis. *Mol Cell Biol* **22**, 4189-4201 (2002).
30 Majsterek, I., Blasiak, J., Mlynarski, W., Hoser, G. & Skorski, T. Does the bcr/abl-mediated increase in the efficacy of DNA repair play a role in the drug

resistance of cancer cells? *Cell Biol Int* **26**, 363-370, doi:10.1006/cbir.2002.0865 (2002).

31 Pytel, D., Wysocki, T. & Majsterek, I. Comparative study of DNA damage, cell cycle and apoptosis in human K562 and CCRF-CEM leukemia cells: role of BCR/ABL in therapeutic resistance. *Comp Biochem Physiol C Toxicol Pharmacol* **144**, 85-92, doi:10.1016/j.cbpc.2006.06.010 (2006).

32 Skorski, T. BCR/ABL regulates response to DNA damage: the role in resistance to genotoxic treatment and in genomic instability. *Oncogene* **21**, 8591-8604, doi:10.1038/sj.onc.1206087 (2002).

33 Nowicki, M. O. *et al.* BCR/ABL oncogenic kinase promotes unfaithful repair of the reactive oxygen species-dependent DNA double-strand breaks. *Blood* **104**, 3746-3753, doi:10.1182/blood-2004-05-1941 (2004).

34 Sattler, M. *et al.* The BCR/ABL tyrosine kinase induces production of reactive oxygen species in hematopoietic cells. *J Biol Chem* **275**, 24273-24278, doi:10.1074/jbc.M002094200 (2000).

35 Melo, J. V. & Barnes, D. J. Chronic myeloid leukaemia as a model of disease evolution in human cancer. *Nat Rev Cancer* **7**, 441-453, doi:10.1038/nrc2147 (2007).

36 Cortes, J. E., Talpaz, M. & Kantarjian, H. Chronic myelogenous leukemia: a review. *Am J Med* **100**, 555-570 (1996).

37 Rassool, F. V. *et al.* Reactive oxygen species, DNA damage, and error-prone repair: a model for genomic instability with progression in myeloid leukemia? *Cancer Res* **67**, 8762-8771, doi:10.1158/0008-5472.CAN-06-4807 (2007).

38 Downward, J. Targeting RAS signalling pathways in cancer therapy. *Nat Rev Cancer* **3**, 11-22, doi:10.1038/nrc969 (2003).

39 Padua, R. A. *et al.* RAS, FMS and p53 mutations and poor clinical outcome in myelodysplasias: a 10-year follow-up. *Leukemia* **12**, 887-892 (1998).

40 Sulkowski, P. L. *et al.* 2-Hydroxyglutarate produced by neomorphic IDH mutations suppresses homologous recombination and induces PARP inhibitor sensitivity. *Sci Transl Med* **9**, doi:10.1126/scitranslmed.aal2463 (2017).

41 Esposito, M. T. *et al.* Synthetic lethal targeting of oncogenic transcription factors in acute leukemia by PARP inhibitors. *Nat Med* **21**, 1481-1490, doi:10.1038/nm.3993 (2015).

42 Inoue, S. *et al.* Mutant IDH1 Downregulates ATM and Alters DNA Repair and Sensitivity to DNA Damage Independent of TET2. *Cancer Cell* **30**, 337-348, doi:10.1016/j.ccell.2016.05.018 (2016).

43 Wang, D., Kreutzer, D. A. & Essigmann, J. M. Mutagenicity and repair of oxidative DNA damage: insights from studies using defined lesions. *Mutat Res* **400**, 99-115 (1998).

44 Irani, K. & Goldschmidt-Clermont, P. J. Ras, superoxide and signal transduction. *Biochem Pharmacol* **55**, 1339-1346 (1998).

45 Cairns, R. A. & Mak, T. W. Oncogenic isocitrate dehydrogenase mutations: mechanisms, models, and clinical opportunities. *Cancer Discov* **3**, 730-741, doi:10.1158/2159-8290.CD-13-0083 (2013).

46 Paschka, P. *et al.* IDH1 and IDH2 mutations are frequent genetic alterations in acute myeloid leukemia and confer adverse prognosis in cytogenetically normal acute myeloid leukemia with NPM1 mutation without FLT3 internal

tandem duplication. *J Clin Oncol* **28**, 3636-3643, doi:10.1200/JCO.2010.28.3762 (2010).

47 Zhao, L. & So, C. W. E. PARPi potentiates with current conventional therapy in MLL leukemia. *Cell Cycle* **16**, 1861-1869, doi:10.1080/15384101.2017.1288325 (2017).

48 Rosnet, O., Mattei, M. G., Marchetto, S. & Birnbaum, D. Isolation and chromosomal localization of a novel FMS-like tyrosine kinase gene. *Genomics* **9**, 380-385, doi:0888-7543(91)90270-O [pii] (1991).

49 Carow, C. E. *et al.* Localization of the human stem cell tyrosine kinase-1 gene (FLT3) to 13q12-->q13. *Cytogenet Cell Genet* **70**, 255-257 (1995).

50 Agnes, F. *et al.* Genomic structure of the downstream part of the human FLT3 gene: exon/intron structure conservation among genes encoding receptor tyrosine kinases (RTK) of subclass III. *Gene* **145**, 283-288 (1994).

51 Griffith, J. *et al.* The structural basis for autoinhibition of FLT3 by the juxtamembrane domain. *Mol Cell* **13**, 169-178, doi:S1097276503005057 [pii] (2004).

52 Lyman, S. D. & Jacobsen, S. E. c-kit ligand and Flt3 ligand: stem/progenitor cell factors with overlapping yet distinct activities. *Blood* **91**, 1101-1134 (1998).

53 Markovic, A., MacKenzie, K. L. & Lock, R. B. FLT-3: a new focus in the understanding of acute leukemia. *Int J Biochem Cell Biol* **37**, 1168-1172, doi:S1357-2725(04)00431-5 [pii]
10.1016/j.biocel.2004.12.005 (2005).

54 Zhang, S. *et al.* Essential role of signal transducer and activator of transcription (Stat)5a but not Stat5b for Flt3-dependent signaling. *J Exp Med* **192**, 719-728 (2000).

55 Grafone, T., Palmisano, M., Nicci, C. & Storti, S. An overview on the role of FLT3-tyrosine kinase receptor in acute myeloid leukemia: biology and treatment. *Oncol Rev* **6**, e8, doi:10.4081/oncol.2012.e8 (2012).

56 Chen, W. *et al.* mTOR signaling is activated by FLT3 kinase and promotes survival of FLT3-mutated acute myeloid leukemia cells. *Mol Cancer* **9**, 292, doi:10.1186/1476-4598-9-292 (2010).

57 Leung, A. Y., Man, C. H. & Kwong, Y. L. FLT3 inhibition: a moving and evolving target in acute myeloid leukaemia. *Leukemia* **27**, 260-268, doi:10.1038/leu.2012.195 (2013).

58 Gale, R. E. *et al.* The impact of FLT3 internal tandem duplication mutant level, number, size, and interaction with NPM1 mutations in a large cohort of young adult patients with acute myeloid leukemia. *Blood* **111**, 2776-2784, doi:10.1182/blood-2007-08-109090 (2008).

59 Meshinchi, S. *et al.* Structural and numerical variation of FLT3/ITD in pediatric AML. *Blood* **111**, 4930-4933, doi:10.1182/blood-2008-01-117770 (2008).

60 Santos, F. P. *et al.* Prognostic value of FLT3 mutations among different cytogenetic subgroups in acute myeloid leukemia. *Cancer* **117**, 2145-2155, doi:10.1002/cncr.25670 (2011).

61 Bagrintseva, K. *et al.* FLT3-ITD-TKD dual mutants associated with AML confer resistance to FLT3 PTK inhibitors and cytotoxic agents by overexpression of Bcl-x(L). *Blood* **105**, 3679-3685, doi:10.1182/blood-2004-06-2459 (2005).

62 Smith, C. C. *et al.* Validation of ITD mutations in FLT3 as a therapeutic target in human acute myeloid leukaemia. *Nature* **485**, 260-263, doi:10.1038/nature11016 (2012).
63 Zhou, J. *et al.* Enhanced activation of STAT pathways and overexpression of survivin confer resistance to FLT3 inhibitors and could be therapeutic targets in AML. *Blood* **113**, 4052-4062, doi:10.1182/blood-2008-05-156422 (2009).
64 Kojima, K. *et al.* p53 activation of mesenchymal stromal cells partially abrogates microenvironment-mediated resistance to FLT3 inhibition in AML through HIF-1alpha-mediated down-regulation of CXCL12. *Blood* **118**, 4431-4439, doi:10.1182/blood-2011-02-334136 (2011).
65 Man, C. H. *et al.* A novel tescalcin-sodium/hydrogen exchange axis underlying sorafenib resistance in FLT3-ITD+ AML. *Blood* **123**, 2530-2539, doi:10.1182/blood-2013-07-512194 (2014).
66 Krokan, H. E., Standal, R. & Slupphaug, G. DNA glycosylases in the base excision repair of DNA. *Biochem J* **325 (Pt 1)**, 1-16 (1997).
67 Neeley, W. L. & Essigmann, J. M. Mechanisms of formation, genotoxicity, and mutation of guanine oxidation products. *Chem Res Toxicol* **19**, 491-505, doi:10.1021/tx0600043 (2006).
68 Grollman, A. P. & Moriya, M. Mutagenesis by 8-oxoguanine: an enemy within. *Trends Genet* **9**, 246-249 (1993).
69 Holmstrom, K. M. & Finkel, T. Cellular mechanisms and physiological consequences of redox-dependent signalling. *Nat Rev Mol Cell Biol* **15**, 411-421, doi:10.1038/nrm3801 (2014).
70 Sallmyr, A. *et al.* Internal tandem duplication of FLT3 (FLT3/ITD) induces increased ROS production, DNA damage, and misrepair: implications for poor prognosis in AML. *Blood* **111**, 3173-3182, doi:10.1182/blood-2007-05-092510 (2008).
71 Woolley, J. F. *et al.* H2O2 production downstream of FLT3 is mediated by p22phox in the endoplasmic reticulum and is required for STAT5 signalling. *PLoS One* **7**, e34050, doi:10.1371/journal.pone.0034050 (2012).
72 Stanicka, J., Russell, E. G., Woolley, J. F. & Cotter, T. G. NADPH oxidase-generated hydrogen peroxide induces DNA damage in mutant FLT3-expressing leukemia cells. *J Biol Chem* **290**, 9348-9361, doi:10.1074/jbc.M113.510495 (2015).
73 Jayavelu, A. K. *et al.* NOX4-driven ROS formation mediates PTP inactivation and cell transformation in FLT3ITD-positive AML cells. *Leukemia* **30**, 473-483, doi:10.1038/leu.2015.234 (2016).
74 Fan, J., Li, L., Small, D. & Rassool, F. Cells expressing FLT3/ITD mutations exhibit elevated repair errors generated through alternative NHEJ pathways: implications for genomic instability and therapy. *Blood* **116**, 5298-5305, doi:10.1182/blood-2010-03-272591 (2010).
75 Farmer, H. *et al.* Targeting the DNA repair defect in BRCA mutant cells as a therapeutic strategy. *Nature* **434**, 917-921, doi:10.1038/nature03445 (2005).
76 Bryant, H. E. *et al.* Specific killing of BRCA2-deficient tumours with inhibitors of poly(ADP-ribose) polymerase. *Nature* **434**, 913-917, doi:10.1038/nature03443 (2005).

77 Yap, T. A., Sandhu, S. K., Carden, C. P. & de Bono, J. S. Poly(ADP-ribose) polymerase (PARP) inhibitors: Exploiting a synthetic lethal strategy in the clinic. *CA Cancer J Clin* **61**, 31-49, doi:10.3322/caac.20095 (2011).

78 Hengel, S. R., Spies, M. A. & Spies, M. Small-Molecule Inhibitors Targeting DNA Repair and DNA Repair Deficiency in Research and Cancer Therapy. *Cell Chem Biol* **24**, 1101-1119, doi:10.1016/j.chembiol.2017.08.027 (2017).

79 Murata, S. *et al.* Predictors and Modulators of Synthetic Lethality: An Update on PARP Inhibitors and Personalized Medicine. *Biomed Res Int* **2016**, 2346585, doi:10.1155/2016/2346585 (2016).

80 Nakao, M. *et al.* Internal tandem duplication of the flt3 gene found in acute myeloid leukemia. *Leukemia* **10**, 1911-1918 (1996).

81 Cortes J, K. S., Martinelli G, et al. in *23rd Congress of the European Hematology Association* (Stockholm, Sweden., June 16, 2018).

82 Perl, A. E. *et al.* Selective inhibition of FLT3 by gilteritinib in relapsed or refractory acute myeloid leukaemia: a multicentre, first-in-human, open-label, phase 1-2 study. *Lancet Oncol* **18**, 1061-1075, doi:10.1016/S1470-2045(17)30416-3 (2017).

83 Wang E, S. R., Collins R, et al. in *2017 EHA Congress* (Madrid, Spain. , 2017).

84 Jorge E. Cortes, H. M. K., Tapan M. Kadia, Gautam Borthakur, Marina Konopleva, Guillermo Garcia-Manero, Naval Guastad Daver, Naveen Pemmaraju, Elias Jabbour, Zeev Estrov, Abhijit Ramachandran, Jamil Paradela, Blake Pond, Farhad Ravandi, Madhuri Vusirikala, Prapti Arvind Patel, Mark J. Levis, Alexander E. Perl, Michael Andreeff, Robert Collins. Crenolanib besylate, a type I pan-FLT3 inhibitor, to demonstrate clinical activity in multiply relapsed FLT3-ITD and D835 AML. *Journal of Clinical Oncology* **34** (2016).

85 Tang, R., Dodd, A., Lai, D., McNabb, W. C. & Love, D. R. Validation of zebrafish (Danio rerio) reference genes for quantitative real-time RT-PCR normalization. *Acta Biochim Biophys Sin (Shanghai)* **39**, 384-390 (2007).

86 Gyori, B. M., Venkatachalam, G., Thiagarajan, P. S., Hsu, D. & Clement, M. V. OpenComet: an automated tool for comet assay image analysis. *Redox Biol* **2**, 457-465, doi:10.1016/j.redox.2013.12.020 (2014).

87 Certo, M. T. *et al.* Tracking genome engineering outcome at individual DNA breakpoints. *Nat Methods* **8**, 671-676, doi:10.1038/nmeth.1648 (2011).

88 Fellmann, C. *et al.* An optimized microRNA backbone for effective single-copy RNAi. *Cell Rep* **5**, 1704-1713, doi:10.1016/j.celrep.2013.11.020 (2013).

89 Milanowska, K. *et al.* REPAIRtoire--a database of DNA repair pathways. *Nucleic Acids Res* **39**, D788-792, doi:10.1093/nar/gkq1087 (2011).

90 Kanehisa, M. & Goto, S. KEGG: kyoto encyclopedia of genes and genomes. *Nucleic Acids Res* **28**, 27-30 (2000).

91 Wunderlich, M. *et al.* AML cells are differentially sensitive to chemotherapy treatment in a human xenograft model. *Blood* **121**, e90-97, doi:10.1182/blood-2012-10-464677 (2013).

92 Lee, B. H. *et al.* FLT3 mutations confer enhanced proliferation and survival properties to multipotent progenitors in a murine model of chronic myelomonocytic leukemia. *Cancer Cell* **12**, 367-380, doi:10.1016/j.ccr.2007.08.031 (2007).

93 Godfrey, R. *et al.* Cell transformation by FLT3 ITD in acute myeloid leukemia involves oxidative inactivation of the tumor suppressor protein-tyrosine phosphatase DEP-1/ PTPRJ. *Blood* **119**, 4499-4511, doi:10.1182/blood-2011-02-336446 (2012).
94 Klein, H. U. *et al.* Quantitative comparison of microarray experiments with published leukemia related gene expression signatures. *BMC Bioinformatics* **10**, 422, doi:10.1186/1471-2105-10-422 (2009).
95 Lam, S. S. *et al.* Homoharringtonine (omacetaxine mepesuccinate) as an adjunct for FLT3-ITD acute myeloid leukemia. *Sci Transl Med* **8**, 359ra129, doi:10.1126/scitranslmed.aaf3735 (2016).
96 Xia, F. *et al.* Deficiency of human BRCA2 leads to impaired homologous recombination but maintains normal nonhomologous end joining. *Proc Natl Acad Sci U S A* **98**, 8644-8649, doi:10.1073/pnas.151253498 (2001).
97 Moynahan, M. E., Pierce, A. J. & Jasin, M. BRCA2 is required for homology-directed repair of chromosomal breaks. *Mol Cell* **7**, 263-272 (2001).
98 Davies, A. A. *et al.* Role of BRCA2 in control of the RAD51 recombination and DNA repair protein. *Mol Cell* **7**, 273-282 (2001).
99 Chen, P. L. *et al.* The BRC repeats in BRCA2 are critical for RAD51 binding and resistance to methyl methanesulfonate treatment. *Proc Natl Acad Sci U S A* **95**, 5287-5292 (1998).
100 Chen, J. *et al.* Stable interaction between the products of the BRCA1 and BRCA2 tumor suppressor genes in mitotic and meiotic cells. *Mol Cell* **2**, 317-328 (1998).
101 Couch, F. J. *et al.* BRCA2 germline mutations in male breast cancer cases and breast cancer families. *Nat Genet* **13**, 123-125, doi:10.1038/ng0596-123 (1996).
102 Wooster, R. *et al.* Identification of the breast cancer susceptibility gene BRCA2. *Nature* **378**, 789-792, doi:10.1038/378789a0 (1995).
103 Gaymes, T. J., Mohamedali, A., Eiliazadeh, A. L., Darling, D. & Mufti, G. J. FLT3 and JAK2 Mutations in Acute Myeloid Leukemia Promote Interchromosomal Homologous Recombination and the Potential for Copy Neutral Loss of Heterozygosity. *Cancer Res* **77**, 1697-1708, doi:10.1158/0008-5472.CAN-16-1678 (2017).
104 Moloney, J. N., Stanicka, J. & Cotter, T. G. Subcellular localization of the FLT3-ITD oncogene plays a significant role in the production of NOX- and p22(phox)-derived reactive oxygen species in acute myeloid leukemia. *Leuk Res* **52**, 34-42, doi:10.1016/j.leukres.2016.11.006 (2017).
105 Mupo, A. *et al.* A powerful molecular synergy between mutant Nucleophosmin and Flt3-ITD drives acute myeloid leukemia in mice. *Leukemia* **27**, 1917-1920, doi:10.1038/leu.2013.77 (2013).
106 Dai, Z. *et al.* edgeR: a versatile tool for the analysis of shRNA-seq and CRISPR-Cas9 genetic screens. *F1000Res* **3**, 95, doi:10.12688/f1000research.3928.2 (2014).
107 Loeb, L. A. & Monnat, R. J., Jr. DNA polymerases and human disease. *Nat Rev Genet* **9**, 594-604, doi:10.1038/nrg2345 (2008).
108 Lange, S. S., Takata, K. & Wood, R. D. DNA polymerases and cancer. *Nat Rev Cancer* **11**, 96-110, doi:10.1038/nrc2998 (2011).

109 Hubscher, U., Maga, G. & Spadari, S. Eukaryotic DNA polymerases. *Annu Rev Biochem* **71**, 133-163, doi:10.1146/annurev.biochem.71.090501.150041 (2002).
110 Zeman, M. K. & Cimprich, K. A. Causes and consequences of replication stress. *Nat Cell Biol* **16**, 2-9, doi:10.1038/ncb2897 (2014).
111 Marechal, A. & Zou, L. DNA damage sensing by the ATM and ATR kinases. *Cold Spring Harb Perspect Biol* **5**, doi:10.1101/cshperspect.a012716 (2013).
112 Magdalou, I., Lopez, B. S., Pasero, P. & Lambert, S. A. The causes of replication stress and their consequences on genome stability and cell fate. *Semin Cell Dev Biol* **30**, 154-164, doi:10.1016/j.semcdb.2014.04.035 (2014).
113 Seedhouse, C. H. *et al.* DNA repair contributes to the drug-resistant phenotype of primary acute myeloid leukaemia cells with FLT3 internal tandem duplications and is reversed by the FLT3 inhibitor PKC412. *Leukemia* **20**, 2130-2136, doi:10.1038/sj.leu.2404439 (2006).
114 Kang, M. A., So, E. Y., Simons, A. L., Spitz, D. R. & Ouchi, T. DNA damage induces reactive oxygen species generation through the H2AX-Nox1/Rac1 pathway. *Cell Death Dis* **3**, e249, doi:10.1038/cddis.2011.134 (2012).
115 Rundle, S., Bradbury, A., Drew, Y. & Curtin, N. J. Targeting the ATR-CHK1 Axis in Cancer Therapy. *Cancers (Basel)* **9**, doi:10.3390/cancers9050041 (2017).
116 Shih, A. H. *et al.* Mutational cooperativity linked to combinatorial epigenetic gain of function in acute myeloid leukemia. *Cancer Cell* **27**, 502-515, doi:10.1016/j.ccell.2015.03.009 (2015).
117 Jayavelu, A. K., Moloney, J. N., Bohmer, F. D. & Cotter, T. G. NOX-driven ROS formation in cell transformation of FLT3-ITD-positive AML. *Exp Hematol* **44**, 1113-1122, doi:10.1016/j.exphem.2016.08.008 (2016).
118 Li, L. *et al.* Knock-in of an internal tandem duplication mutation into murine FLT3 confers myeloproliferative disease in a mouse model. *Blood* **111**, 3849-3858, doi:10.1182/blood-2007-08-109942 (2008).
119 Mallardo, M. *et al.* NPMc+ and FLT3_ITD mutations cooperate in inducing acute leukaemia in a novel mouse model. *Leukemia* **27**, 2248-2251, doi:10.1038/leu.2013.114 (2013).
120 Behrens, K. *et al.* RUNX1 cooperates with FLT3-ITD to induce leukemia. *J Exp Med* **214**, 737-752, doi:10.1084/jem.20160927 (2017).
121 Meyer, S. E. *et al.* DNMT3A Haploinsufficiency Transforms FLT3ITD Myeloproliferative Disease into a Rapid, Spontaneous, and Fully Penetrant Acute Myeloid Leukemia. *Cancer Discov* **6**, 501-515, doi:10.1158/2159-8290.CD-16-0008 (2016).
122 Yang, L. *et al.* DNMT3A Loss Drives Enhancer Hypomethylation in FLT3-ITD-Associated Leukemias. *Cancer Cell* **29**, 922-934, doi:10.1016/j.ccell.2016.05.003 (2016).